Doctoral Dissertation

Development of Innovated Strategy to Prepare Carbon-Supported Metal Nanoparticles Based on Ionic Liquid-Sputtering Method and Its Application to High-Performance Electrocatalysts Preparation

Tomoya Sasaki

June 2021

Department of Applied Chemistry

Graduate School of Engineering,

Osaka University

Development of Innovated Strategy to Prepare Carbon-Supported Metal Nanoparticles Based on Ionic Liquid-Sputtering Method and Its Application to High-Performance Electrocatalysts Preparation

(イオン液体 - スパッタリング法をベースとした炭素担持金属ナノ粒子を調製する革新的手法の開発とその高性能電極触媒調製への応用)

2021

Tomoya Sasaki

Department of Applied Chemistry

Graduate School of Engineering

Osaka University

Preface

The studies of this doctoral thesis were carried out under the guidance of Professor Dr. Susumu Kuwabata at Department of Applied Chemistry, Graduate School of Engineering, Osaka University during 2015-2021.

The object of this thesis is to develop the preparation method of carbon-supported Pt nanoparticles catalyst with high catalytic activity and durability using Pt nanoparticle-dispersed ionic liquid prepared by “the ionic liquid-sputtering method” aiming at fabrication of high performance cathodes for the fuel cells. For this purpose, the nanoparticle formation during “the ionic liquid-sputtering method” and adsorption of Pt nanoparticles in ionic liquids onto carbon have been analyzed in detail. The author hopes that the preparation method developed in this thesis would contribute to progress science and technology in the fields of ionic liquid and fuel cell catalyst.

Tomoya Sasaki

Department of Applied Chemistry,

Graduate School of Engineering,

Osaka University

Suita, Osaka,

Japan

January, 2021

Contents

General Introduction

Metal nanoparticles (NPs) have attracted much attention as functional materials used in various fields such as optical devices,[1-3] catalysts,[4-6] and sensors[7-9] because of their unique properties generated by the confined tiny quantum structure. Miniaturizing metals to a few nanometers bring about appearance of specific properties including large surface area, melting point depression,[10] quantum size effect[11] and high catalytic activities[4-6] due to a large fraction of the NP's atom lies in the surface and the properties of that surface layer dominate over those of the bulk material. Among metal NPs, Pt NP has been applied to polymer electrolyte fuel cell (PEFC) due to high catalytic activities against the oxygen reduction reaction (ORR).

Background of Pt-C electrocatalysts for PEFC

In 2020, governments of major nations of the world declared prohibition of new gasoline vehicle sales in near future. While most of nations will implement it by the 2030s, Norway government has surprisingly declared the ban by 2025. On December 3rd, 2020, Japan government also announced the ban on sale of gasoline vehicles by the 2030s. As the world-wide transition of CO_2 emission free vehicles accelerates, expectations of PEFC heighten as a promising energy generator for a sustainable vehicle. However, use of Pt, which is the rarest elements in Earth's crust, as catalyst for PEFC has become an issue to be solved from an elemental strategic point of view. From economical viewpoints, a non-platinum electrocatalyst is a subject to be researched but it is not yet practical because of its too low power density,[12] and amelioration of carbon-supported Pt nanoparticles (Pt-C) is still of importance to solve remaining issues such as decrement of Pt usage, enhancement of catalytic activity, and prevention of deterioration. Therefore, researchers around the world have devoted tremendous efforts to improve the efficiency of the Pt-C in PEFC. [13-21] Especially, in the strategic road map

for hydrogen and fuel cells 2019 of Japan, the goal is to reduce the price of fuel cell vehicles (about 7.1 million yen in 2020, TOYOTA MIRAI) to the same price as electric vehicles (about 3.3 million yen in 2020, Nissan LEAF) up to 2025.

The carbon-supported Pt based NP is generally used as cathode electrocatalyst in PEFC. They are mainly prepared by an impregnation method[22-24] and a colloid method.[25, 26] In the former method, the carbon-supported Pt NP is prepared by chemical reduction of Pt precursors adsorbed on carbon powder. Although this method fits to mass-production, it is relatively hard to control the particle size and distribution. The latter method is immobilization of Pt NPs with a surface stabilizer on their surfaces onto carbon material. The particle size and distribution are homogeneously controllable due to the surface stabilizer, but the stabilizer molecules adsorbed interfere with the ORR.[27] Therefore, a novel preparation method which overcome these issues is awaited.

Preparation of metal nanoparticles with room temperature ionic liquid

Room-temperature ionic liquid (RTIL) or simply ionic liquid (IL) is a liquid salt consisting entirely of cations and anions at room temperature and is a subset of a molten salt. Since the IL has a lot of unique properties such as negligible vapor pressure, a wide electrochemical window, good thermal stability, and antistatic properties, they have been applied to a variety of field.[28-37] The history of the ILs began since 1912 when the first room-temperature molten salt (melting point < 298 K), ethylammonium nitrate, was found by Paul Walden.[38] At that time, there was no word of "ionic liquid" and didn't receive much attention. In 1982, C. L. Hussey et al. named chloroaluminate-based room temperature molten salts "ionic liquid".[39] However, it was difficult to handle them because they react violently with moisture in air. The origin of the current active research is a report published by J. S. Wilkes et al. in 1992.[40] They found several ILs represented by 1-ethyl-3-methylimidazolium tetrafluoroborate ($[C_2mim][BF_4]$), which are room temperature molten salts with non-volatiles and stable under air. As it became much easier

to handle ILs, the ILs have become attracting much attentions of many researchers.

Recently, the IL has been recognized as an excellent medium for synthesis of metal NPs because it can stabilize metal NP surface, producing homogeneously size-dispersed NPs without any surface stabilizer.[41-43] The first discovery of this significant function was reported in 2002 as for preparation of Ir NP by chemical reduction in 1-butyl-3-methylimidazoilum hexafluorophosphate ([C_4mim][PF_6])[44] and that of Ge NP by electrochemical reduction in [C_4mim][PF_6].[45] Besides such the function, the extremely low vapor pressure of ILs allows analyses of the prepared samples by devices which need ultra-vacuum condition like X-ray photoemission spectroscopy (XPS)[46-49] and electron microscope.[50-53] In 2006, T. Torimoto and S. Kuwabata et al. published a paper concerning development of a method to synthesize metal NPs by direct magnetron sputter-deposition onto IL under low pressure (Figure 1).[54] Later, this method, which they named "ionic liquid-sputtering method", was found to make it possible to prepare various metal and metal oxide NPs just by replacing the target metal with other kinds of metals.[55-61] Unrequisite of any additives such as precursors, reducing agents and surface stabilizers is desirable for production of "naked" NPs, which don't have a chemical bonding between a stabilizer and a surface of NP and are stabilized by solvation of IL. As a matter of fact, the "naked" Au NP prepared by this method showed high efficiency and selectivity of hydrogenation.[62, 63] The factors affecting particle size and distribution were extensively investigated by changing temperature of target and ionic liquid, sputtering voltage and current, and structure of anion and cation.[64-69] However, NPs generation process during sputter depositing remains still unclear.

Figure 1. Schematic diagram of procedure for ionic liquid-sputtering method.

Preparation of Pt-C electrocatalysts for PEFC using IL

In 2012, Yoshii et al. found that Pt NPs were immobilized on carbon materials, including single-walled carbon nanotube (SWCNT) with inert surface, by agitating a mixture of carbon materials and Pt-NPs-dispersed IL prepared by the ionic liquid-sputtering method at or over 573 K and that the resulting supported-carbon Pt NPs showed high catalytic activity with high stability toward the ORR.[70, 71] It was demonstrated that a small amount of the existing IL between the Pt NPs and the carbon material suppresses carbon corrosion and improves the immobilization of Pt NPs on the surface of pristine carbon materials (Figure 2). Among ILs, quaternary ammonium based ILs enabled Pt NPs to immobilize on carbon materials, but imidazolium cation based ILs didn't do.[70] However, the detailed immobilization mechanism has not yet been elucidated.

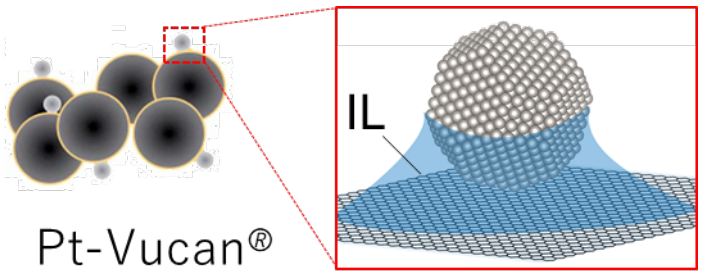

Figure 2. Schematic image of Pt NP immobilized on Vulcan (carbon black) with IL.

Recently, the laboratory, which I belong to, reported that carbon-supported Pt NPs prepared by agitating a mixture of Pt NPs-dispersed IL, carbon material and electropolymerizable compound showed much higher catalytic activity and durability than commercial Pt/C. Careful investigation revealed that the compound in a thin IL was electropolymerized to give the conductive polymer network, which improved electron transfer between Pt NPs and carbon support.[72, 73] This strategy effectively works when using diphenyl amine, methylthiophene and aniline as additives, but use of some other additives regrettably resulted in a failure; pyrrole and 3,4-ethylenedioxythiophene, the latter of which is one of the ideal conducting polymers, were decomposed when heated to induce Pt-NPs adsorption.

The present work

The “ionic liquid-sputtering method” has been developed in the laboratory which I belong to and it was applied to several metal NPs catalysts with high performances, especially to carbon-supported Pt NPs for the ORR. Although catalytic activities have been successfully improved but there remain several matters to be revealed for further improvement of the catalysts as well as for further development of novel catalysts as aforementioned. Under such the background, I started my research work, focusing on development of an innovative preparation method of high-performance electrocatalyst through understanding of unclarified matters with sophisticated techniques.

This thesis consists of three chapters as follows:

Chapter 1 describes operando observation of Au nanoparticle formation during sputter depositing onto IL. The effect of convection during sputter depositing on the size of the resulting nanoparticles was discussed.

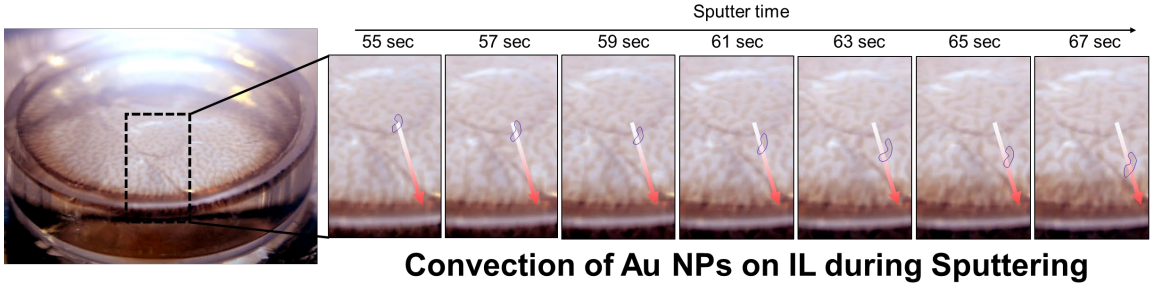

Convection of Au NPs on IL during Sputtering

Chapter 2 describes results obtained by investigation on adsorption behavior of Pt NPs on carbon materials that are coated with ionic liquid. It was found that the adsorption was driven

by electrostatic force between negative-charged Pt NP and positive-charged carbon. No electronically interaction between Pt NP and carbon has been revealed by electrochemical analysis, suggesting that IL worked as nano-glue between Pt NP and carbon support.

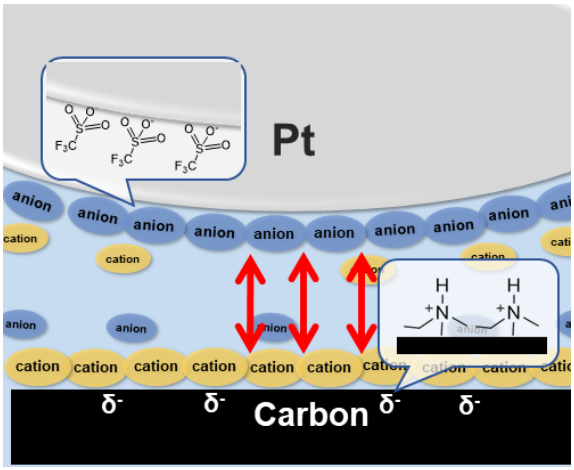

Chapter 3 describes catalytic activity evaluation of the carbon-supported Pt NPs prepared by the method given in chapter 2. The Obtained electrocatalysts showed 2.5 times higher ORR activity than commercial electrocatalyst. Surprisingly, catalytic activity of SWCNT-supported Pt NPs slightly improved after durability test.

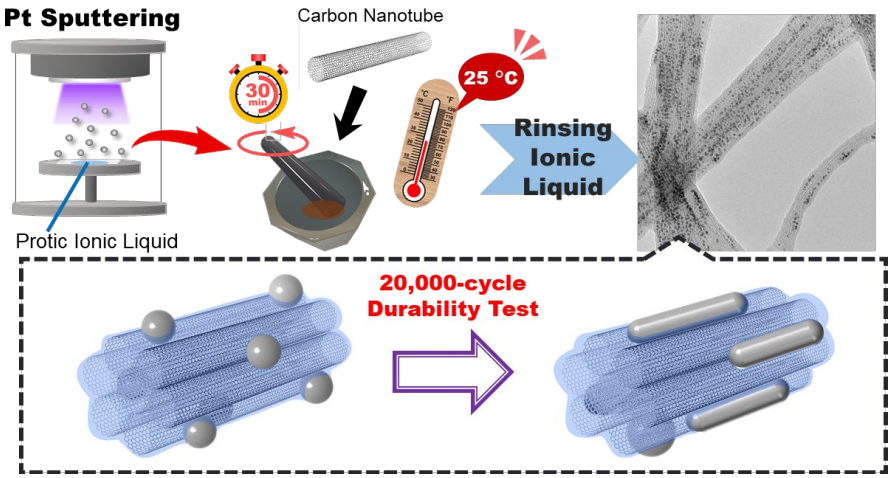

Chapter 4 describes effect of 3,4-ethylenedioxythiophene (EDOT) as additive, which is electropolymerized to high conductive poly-EDOT (PEDOT), on improving catalytic activity. The EDOT in IL between Pt NP and carbon support was electropolymerized, and the resulting polymer enhanced an electric contact between them.

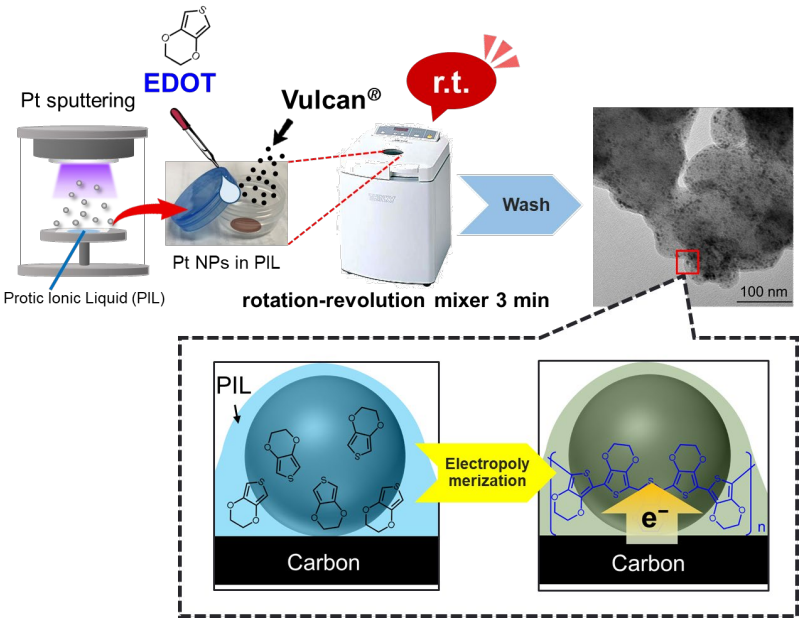

Chapter 1

Operando Observation of Gold Sputtering onto Ionic Liquid

1-1. Introduction

Various kinds of metal or metal oxide nanoparticles (NPs) were prepared by ionic liquid-sputtering method so far.[55-61] In the first report of ionic liquid-sputtering method, the particle size of Au NP were dependent on the structure of ILs. After the report, various researchers have reported the particle size and its distribution of metal NPs prepared by sputtering onto a variety of ILs. However, the values have not been consistent even when the same IL was used. It indicates that the particle size depends on many complicating interrelated factors. In order to identify the factors that have effects on the particle size and its distribution, some systematic studies have been reported and it was concluded that the temperature of the target, the applied voltages, the temperature of the IL and the structure of cation and anion of IL strongly influence the size of the Au NPs (Figure 1-1). [64-69] Although the particle size was controllable by determining the arbitrary value of these factors, the process of the effects on growing particle size was still unclear. About the process, one proposed that metal atoms and clusters generated by bombardment of the metal target due to energetic gas ions are aggregated on the IL surface before their sinking in the IL. It is, however, very hard to observe process of such the events by a microscope in a constrained sputtering chamber.

Although metal clusters and NPs are inherently invisible by naked eyes, gold is exception because Au clusters (< 2-3 nm) exhibit dark color due to quantized electronic energy structure, [74] whereas Au NPs (> 4 nm) gives vivid colors due to plasmon absorption, wavelength of which is dependent on their sizes. As a matter of fact, when gold sputtering on an IL was conducted, appearance and move of colored patterns were realized on the IL surface through a glass

window, letting us notice a possibility to acquire information from the vacuum-IL interface without any specific microscopy devises. It was then attempted to capture the IL during sputtering by a camcorder and the growth process of particle on surface of IL was investigated. From this observation, it was found that Au NP generated on IL surface was diffused by convection of IL.

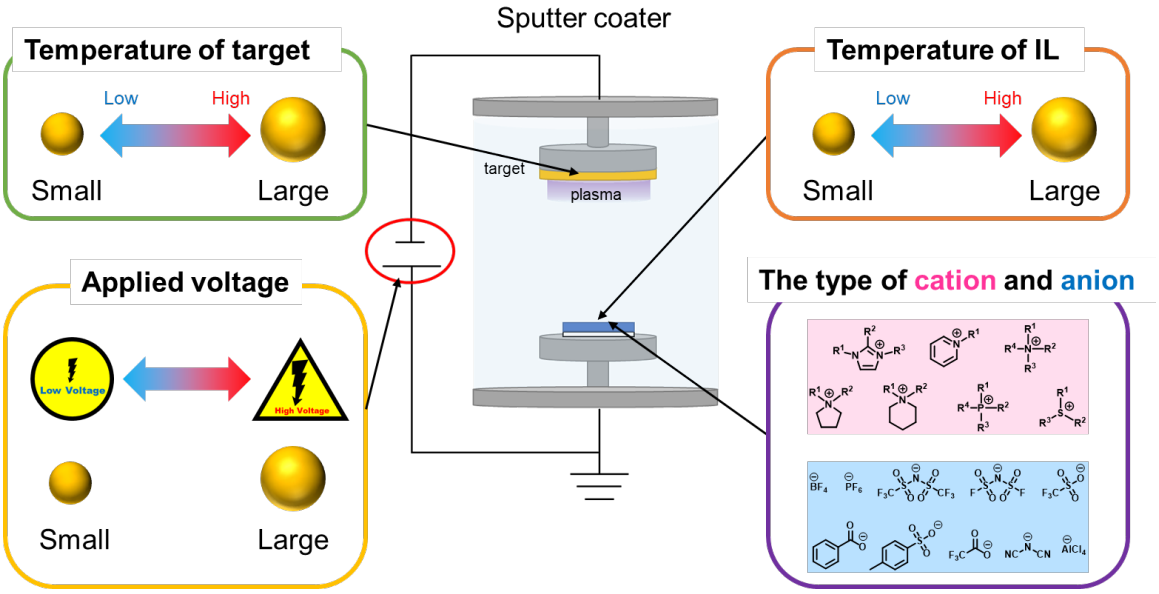

Figure 1-1. Schematic illustration of the factors that have influence on particle size and its distribution.

1-2. Experimental section

1-2-1. Preparation of IL

1-Butyl-3-methylimidazolium chloride ([C_4mim]Cl; Kanto Chemical Co., Ltd.) and lithium bis(trifluoromethanesulfonyl)amide (Li[TFSA]; Morita chemicals Co., Ltd.) were mixed thoroughly in ultrapure water at ambient temperature, then [C_4mim][TFSA] was extracted by dichloromethane, followed by purification with ultrapure water several times.

1-2-2. Operando observation of vacuum and liquid interface during Au sputtering

Figure 1-2(a) shows a schematic illustration of an apparatus for capturing gold sputtering onto [C_4mim][TFSA]. The two kinds of soda glass cups (ϕ13.5 mm, depth 8.0 mm; ϕ27 mm, depth 8.0 mm) were used. A glass cup filled with [C_4mim][TFSA] was put in a magnetron DC sputtering instrument (Cressington108 auto SE coater). A gold target was placed on 32 mm above the top of the cup. Gold sputtering onto [C_4mim][TFSA] was conducted with sputter current of 40 mA for 5 min in dry Ar atmosphere at 5 Pa and the images were recorded in real time by a digital camcorder (Nikon Digital Camera D7100).

Figure 1-2(b) illustrates an experimental apparatus for capturing the surface of an IL thin layer during gold sputtering. A round glass plate (ϕ30 mm), on which [C_4mim][TFSA] (450 μL) was spread, was put on a glass stage with a mirror fixed at 45° beneath the stage in a sputtering instrument (SANYUELECTRON SC-701HMC II). A gold target was placed on 40 mm above the glass stage. Au sputtering onto [C_4mim][TFSA] was conducted with 40 mA and about 700 V under Ar gas at 5 Pa. The IL surface was captured from the bottom through the mirror with the same digital camcorder.

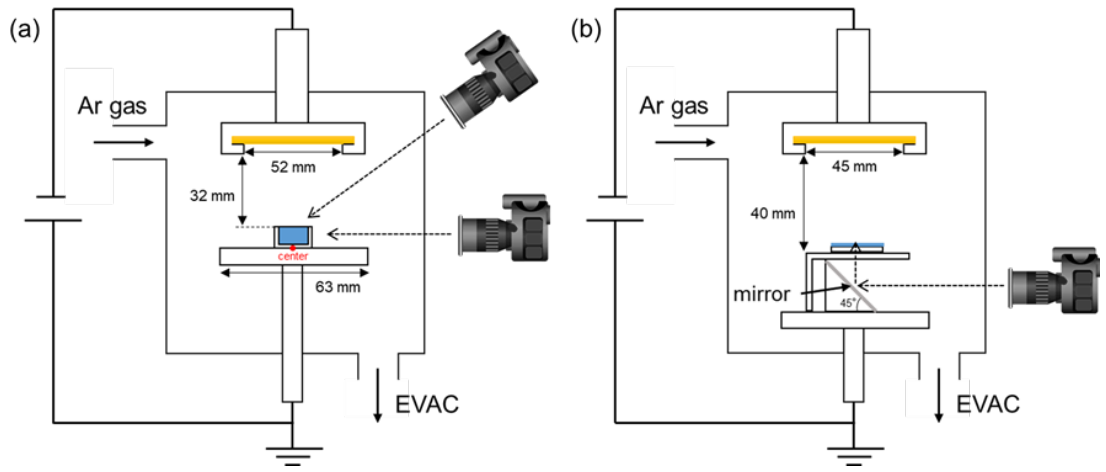

Figure 1-2. Schematic illustration of experimental apparatus for (a) observation of sputtering onto ionic liquid in in a transparent glass cup and (b) ionic liquid thin layer spread on a glass plate.

1-2-3. Transmission electron microscope observation

The transmission electron microscope (TEM) images of the prepared Au NPs were taken by a

Hitachi H-7650 TEM operated at 100 kV. A TEM sample was prepared by dropping 5 μL of the IL subjected to sputtering onto a TEM grid (ϕ 3.0 mm, copper, 400 mesh), followed by softly washing with acetonitrile to remove excess IL.

1-3. Results and discussion

1-3-1. Operando observation of Au sputtering onto ionic liquid in a cup

Figure 1-3 shows frames picked from movies taken by the way shown in Figure 1-2(a) while conducting Au sputtering onto [C_4mim][TFSA]. The side view of the cup and the surface of IL were taken. When Au sputtering began, powder-like brown materials homogeneously appeared on the entire surface of IL and they radiated outward. The observed tiny materials were confirmed to be Au clusters by spectroscopy and TEM observation (see Figure 1-4) of the IL after the Au sputtering. In order to show more clearly the move of the Au clusters on IL with time, magnified pictures of the IL surface are given in Figure 1-5. The contrast of each picture was increased by an imaging software to make spots formed by Au clusters be clearly recognized. Dashed line circles and scale bars are given in each picture to indicate how two spots moved with time. As these pictures show, two spots moved ca. 3 mm for 10 sec, giving its velocity of 0.3 mm s^{-1}. The diffusion coefficient (D) of [C_4mim][TFSA] having 50 cP of viscosity is estimated to be 2.91×10^{-12} m^2 s^{-1} by the Stokes-Einstein relation with the Stokes radius of 1.5 nm that is a half of the average diameter (ca. 3 nm) of Au clusters estimated from a TEM image given in Figure 1-4. If it is assumed that a concentration gradient is as high as 1 mol L^{-1}/cm (= 1×10^5 mol m^{-4}), the Fick's laws of diffusion gives a flux (f) of 2.91×10^{-7} mol m^{-2} s^{-1}. When a substance with a concentration of c [mol m^{-3}] moves in a certain direction at a velocity of v [m s^{-1}], the flux is defined as $f = c\,v$. Then, c = 1000 mol m^{-3} and $f = 2.91\times10^{-7}$ mol m^{-2} s^{-1} give $v = 2.91\times10^{-7}$ mm s^{-1}. Apparently this value is much smaller than the velocity of the spot of Au clusters estimated from pictures given in Figure 1-5.

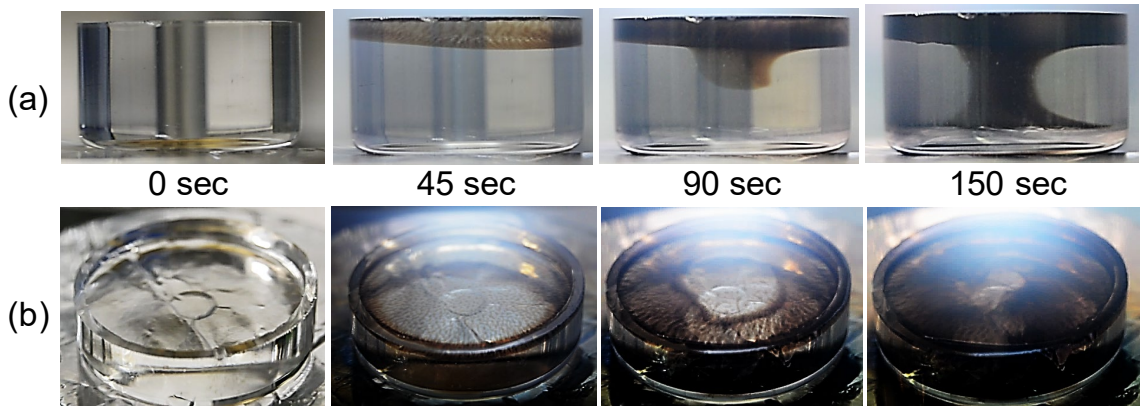

Figure 1-3. Frames picked from movies of (a) the side view of a cup and (b) the surface of IL taken while conducting Au sputtering.

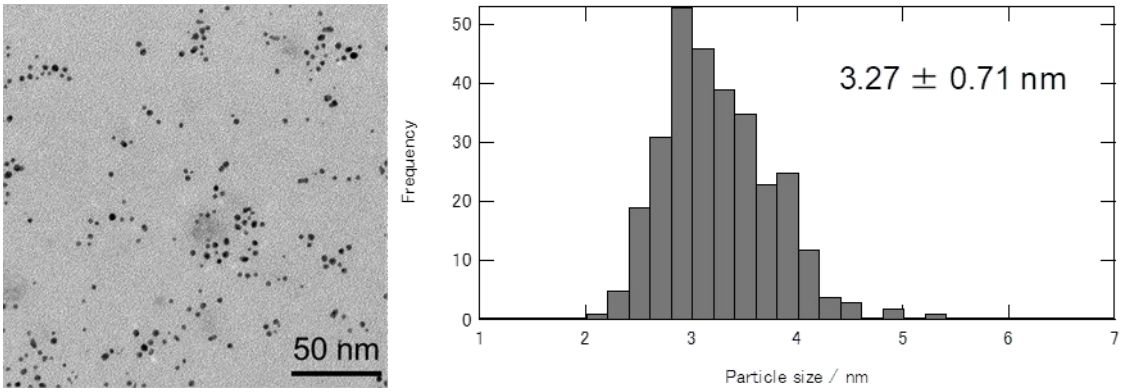

Figure 1-4. TEM image and their size distribution histogram of Au nanoparticles prepared by sputtering onto [C_4mim][TFSA] in glass cup (ϕ13.5 mm, depth 8.0 mm) for 5 min.

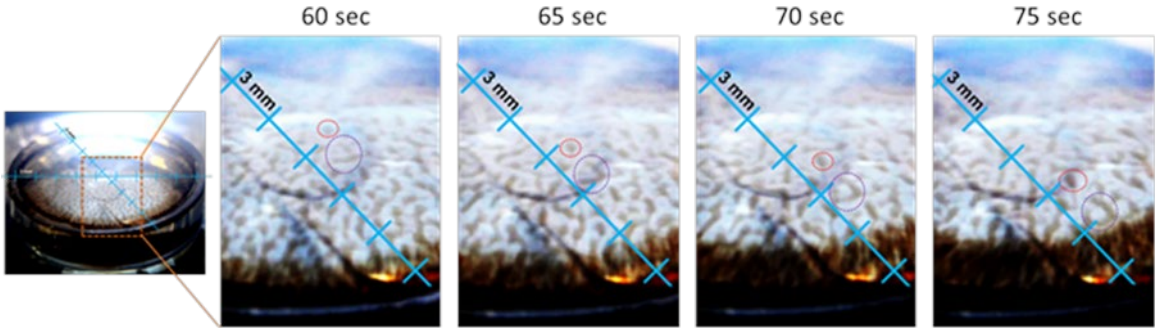

Figure 1-5. Frame picked from movie after 60 seconds, and expanded four pictures taken at 5 seconds interval. Two dashed line circles track the same spots of brown materials derived from Au clusters.

It is then quite natural to ascribe the move of Au clusters with very high speed at vacuum-liquid interface to occurrence of convection of IL during sputtering. Thermal convection of liquid, which is called the Rayleigh-Bénard convection,[75] is well known and its driving force is change in the liquid density by heating, generating convection in a vertical direction. The difference in temperature also causes change in surface tension. Increase in temperature lessens surface tension, producing a driving force for convection in a horizontal direction at the liquid surface from hot area to cold area. This is called the Marangoni convection. Therefore, the move of Au clusters observed at the surface of IL must indicate occurrence of the Marangoni convection during Au sputtering. In general, magnitude of plasma energy in a magnetron sputtering instrument is highest at the center of a target and it decreases toward the periphery. This might make the temperature gradient on the IL surface, which induces the observed convection.

When the Au clusters reached to the wall of the grass cup, they changed their direction toward the center of the cup and moved ca. 5 mm beneath the IL surface. The side view and the surface pictures taken at 45 sec in Figure 1-3 show the first reaching of the Au clusters to the wall. Then, their returning to the center may be recognized by comparing the pictures taken at 45, 90, and 150 sec. Based on the observed fact, the convection flow routes depicted by white arrows in Figure 1-6 seem to be appropriate. Such the behavior is very interesting because the Au clusters arriving at the wall of the cup can take other directions like downward convection but they took the horizontal movement with the opposite direction. Although further investigation is needed to clarify occurrence of the observed convection, it may be one of the reasons that the viscosity of IL at around surface could be decreased by the aforementioned increment of temperature during the sputtering.

Continuous supply of Au clusters and their moving due to the circular convection gathered Au clusters at the center where the liquid density should increase. As a result, downward move

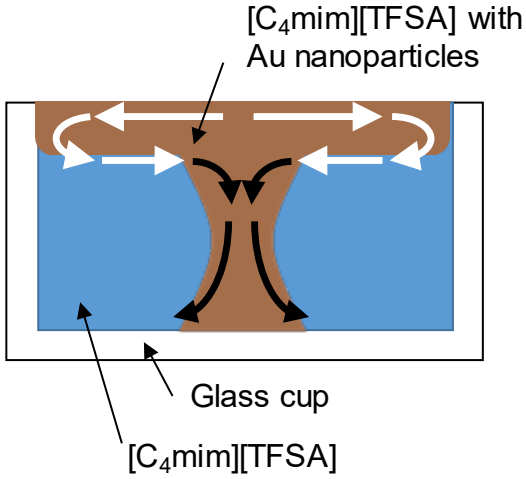

Figure 1-6. Schematic illustration of convections of ionic liquid caused by the Au sputtering. The arrows given in the figure show directions of the convections.

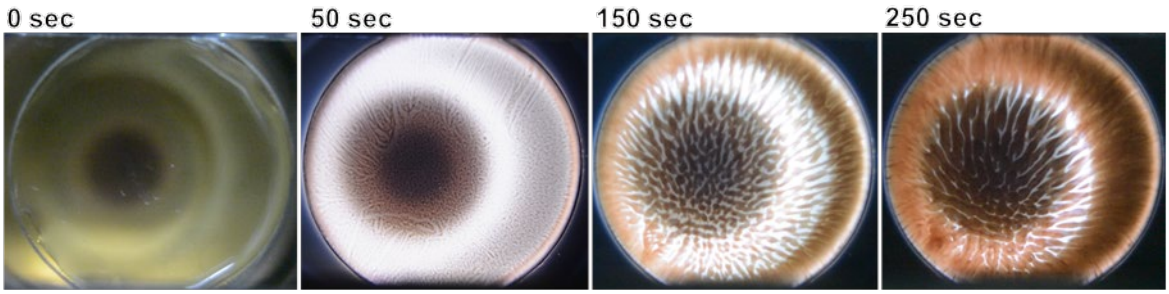

Figure 1-7. Frames picked from a movie of surface of a [C4mim][TFSA] thin layer taken while conducting Au sputtering.

occurred as recognized from the side view pictures taken at 90 and 150 sec in Figure 1-3 (a). This could indicate generation of another convection but the measurement was unfortunately too short to know the whole aspect of the convection. However, according to the well-known fact that a convection takes circular flow, the black solid and broken arrows given in Figure 1-6 can be speculated as the lower convection.

As already mentioned, Au clusters formed spots, which made patchy pattern as recognized from Figure 1-4. The obtained patterns resemble the spinodal decomposition patterns caused by biphasic segregation reaction. In this sputtering method, the IL surface keeps high concentration of Au clusters because it is always supplied with gold clusters during sputtering.

It is known that colloid solution undergoes phase separation when the particle volume fraction becomes very high.[76] The same reason seems to be responsible for the formation of the patchy pattern, but the detailed origin is unknown at present.

1-3-2. Operando observation of Au sputtering onto a thin ionic liquid layer

In order to obtain metal NPs of high concentration, the preparation of NPs has been indeed done by the metal sputtering onto a thin IL layer on a glass plate. Since [C_4mim][TFSA], grass plate, and glass stage are transparent, the image of IL surface could be captured from the backside using a mirror fixed at 45°. Three frames picked from the obtained movie are arrayed in the order of sputtering time in Figure 1-7. The move and the patchy pattern of Au clusters revealed that the convection from the center in a radial fashion occurred in this case as well. Also Au clusters moved toward the center when they reached periphery. Figure 1-8 schematically illustrates the convection in this case.

When metal sputtering is conducted on to IL in a cup, the center portion where Au clusters are gathering can move toward the bottom. In the case of the IL thin layer, however, they don't have no choice but to go up to the surface again, as illustrated in Figure 1-8. Unfortunately, such the move was not able to be observed because high concentration of Au clusters prevented clearly seeing the convection. Instead it was observed the resulting Au clusters by TEM. The

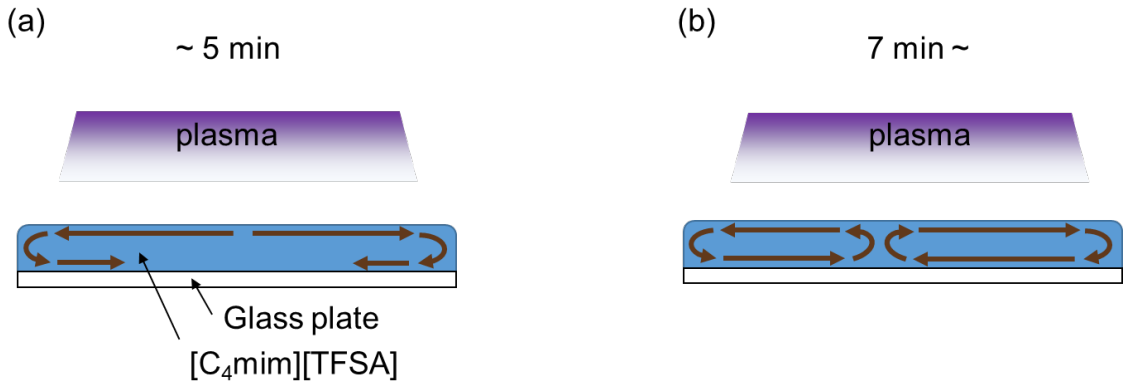

Figure 1-8. Schematic illustration of the convection caused by Au sputtering time for ca. 5 min and ca. 7 min.

obtained images are shown with their size distribution histograms in Figure 1-9. The sample prepared by 3min-sputtering showed size distribution giving one-centered distribution with 2.84 nm of average and 0.59 nm of deviation. However, as the sputtering time was longer, the size distribution separated and became two-centered distribution. The obtained change let us confirm the convection schematically shown in Figure 1-8. Au metal species generated at the Au target in the sputter instrument fall down to the IL surface. The Au clusters located just at the interface can grow due to additionally supplied Au species but the Au clusters located beneath the surface cannot get Au supply. It is, therefore, thought that Au clusters freshly generated at the interface give the size distribution around 2 nm and that Au clusters appeared at the interface again get additional Au supply, becoming Au NPs giving the second size distribution around 4 nm. Adequacy of this assumption is confirmed by the fact that the second size distribution appeared for the sample subjected to sputtering for longer than 7 min, at which it was observed by naked eyes accession of the Au clusters to the center.

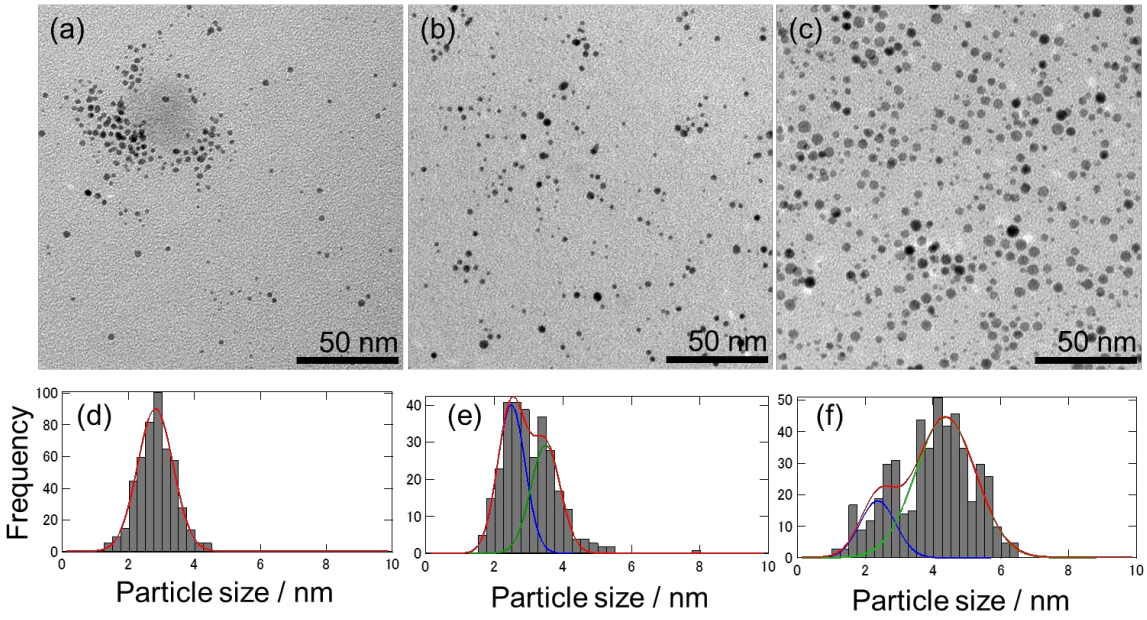

Figure 1-9. TEM images and their size distribution histograms of Au nanoparticles prepared by sputtering for (a,d) 3, (b,e) 10, and (c,f) 15 min.

1-4. Conclusions

It has been speculated that the NPs prepared by the metal sputtering on IL simply proceeds in the following steps so far; generation of Au species by sputtering and their falling onto IL sedimentation of the grown Au NPs. However, the operando observation of the vacuum-IL interface while conducting sputtering revealed move of Au clusters by IL convection plays important role for growth of Au NPs. It has never been considered that the convection is dominant in mass transport of Au cluster, and sputter condition and physicochemical properties of ionic liquids like viscosity has influence this convection. One has to take account into this convection as a factor of Au NPs growth.

Chapter 2

Effect of Ionic Liquid on Adsorption of Pt Nanoparticle onto Carbon Material

2-1. Introduction

Carbon-supported Pt or Pt-alloy nanoparticles are still the best catalysts for polymer-electrolyte fuel cells (PEFCs). This is because the sluggish oxygen reduction reaction (ORR) of the PEFCs requires particularly high Pt loads, although many attempts have been made to develop non-precious-metal catalysts because of the price and the preference for abundant resources.[77-80] It is, however, known that even carbon-supported metal catalysts with sufficient activity suffer from stability issues that are mainly caused by the corrosion of the carbon support, which detaches the metal nanoparticles, and by particle growth due to sintering.[81, 82] To overcome such issues, choosing a carbon support with high durability is one key strategy, and a carbon nanotube (CNT) composed of sp^2 carbons is a promising candidate because it has an extremely inert surface that prevents the corrosion.[83-88] Metal catalyst deposition is possible even on such an inert surface by chemical means, but a weak interaction allows metal particles to easily migrate, resulting in particle growth.[89-92] To firmly fix the metal catalyst, it is necessary to pretreat the surface of the CNT, for example, through the chemical generation of functional groups[93-95] and polymer modification,[96-98] both of which are conducted to create scaffolds to anchor the metal particles. However, it is important to note that the former is accompanied by the partial destruction of the sp^2 structure, which sacrifices the intrinsic stability of the CNT.

In the last decade, using ionic liquid (IL), which has an extremely low vapor pressure, we have developed brand-new methods for preparing metal nanoparticles (NPs), one of which is a combination of dry and wet processes in which metal sputtering is conducted on IL under

reduced pressure.[54, 57, 60] This method, which we call the IL-sputtering method, readily produces several kinds of metal NP with a narrow size distribution. The unique characteristic of the prepared metal NP-dispersed IL is its ability to immobilize the metal NPs on the surfaces of all types of carbon materials, including sp^2-carbon materials such as CNT and highly oriented pyrolytic graphite, just by mixing the liquid and the carbon material, followed by heating at 200°C–300°C.[70, 71, 99] The carbon-supported Pt NPs (Pt-carbon) thus prepared exhibit highs catalytic activity toward an ORR equal to that of the commercial Pt–carbon (Pt–C) catalyst and its durability decidedly surpasses that of the Pt–C even when an untreated single-walled carbon nanotube (SWCNT) is selected as the carbon support. The electrochemical and chemical examinations of the prepared catalysts that we have conducted so far have revealed that quite small amounts of IL function as an adhesive bond for Pt-NP adsorption. It is, however, still unclear how IL behaves to induce spontaneous Pt-NP adsorption during agitation with heating and how Pt NPs adsorbed on the inert CNT surface achieve high durability against an ORR. We initiated the present study with the aim of collecting chemical information to gain a deeper insight into the figuration of the Pt–C catalyst with the aid of IL.

As for the spontaneous adsorption of colloid onto a substrate in the liquid phase, hetero-aggregation caused by electrostatic attraction is generally considered the driving force.[100, 101] To verify whether this possibility is applicable in the case of Pt-NP-dispersed IL and CNTs, zeta potential measurements of IL-modified CNTs were conducted. The results obtained allowed for predictions that provided the possibility of preparing a CNT-supported Pt-NP (Pt-CNT) catalyst without heating if protic IL was used. On the basis of this fascinating finding, we have developed the simplest method containing only sputtering and mixing procedures to fabricate the Pt-CNT catalyst while clarifying the fine structure of the catalyst by electrochemical, electron microscopic, and spectroscopic means.

2-2. Experimental section

2-2-1. Preparation of ionic liquids

Diethylmethylammonium hydrogen sulfate ([dema]HSO_4), [dema][TfO], and diethylmethylammonium bis(trifluoromethanesulfonyl)amide ([dema][TFSA]) were, respectively, synthesized by stoichiometrically adding H_2SO_4 (Wako Pure Chemicals), trifluoromethanesulfonic acid (H[TfO], Tokyo Chemical Industry), and bis(trifluoromethanesulfonyl)amide (H[TFSA], Morita Chemical Industries) to *N,N*-diethylmethylamine (Wako Pure Chemicals) aqueous solution, followed by removal of water at 333 K under vacuum. 1-Butyl-3-methylimidazolium trifluoromethanesulfonate ([C_4mim][TfO]) was prepared by an anion-exchange reaction. [C_4mim]Cl (Tokyo Chemical Industry) and Ag[TfO] (Aldrich) were mixed thoroughly in ultrapure water (Milli-Q water) at ambient temperature to yield [C_4mim][TfO]. The resulting solution was then filtered through a 0.1 μm filter to remove AgCl and dried at 343 K under vacuum for 12 h. The chemical structures of prepared ILs are shown in Figure 2-1.

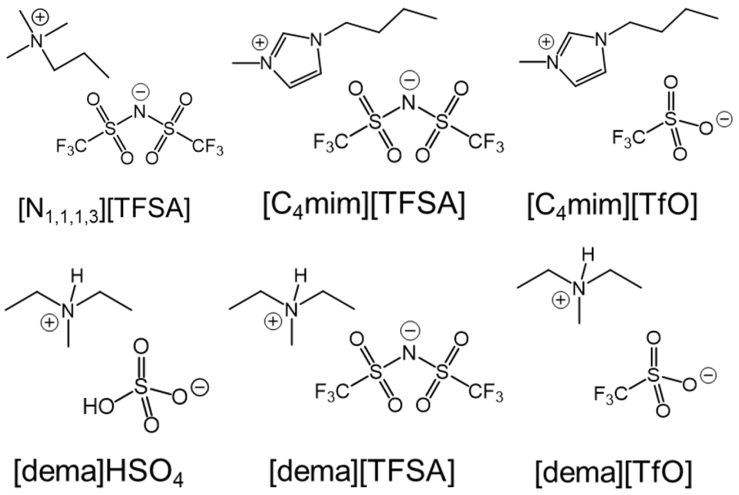

Figure 2-1. Chemical structures of the used ILs.

2-2-2. Preparation of CNT-supported Pt NPs electrocatalysts

Figure 2-2 represents the procedure for the preparation of Pt–CNTs. First, Pt NPs dispersed

in IL (Pt–NP–IL) were prepared using the IL-sputtering method, as follows[102]: 400 μL of IL was put on a soda glass (2.5 cm × 2.5 cm) and spread across the entire surface of the glass, and the glass was then placed in a DC magnetron-sputtering system (Quick Coater SC-701HMCII, Sanyu Electron Co., Ltd.). Pt sputtering was carried out at a current of 40 mA and an applied voltage of 0.7 kV for 15 min under argon conditions of 5 Pa. The ILs used for this purpose were [dema]HSO_4, [dema][TfO], [dema][TFSA], [C_4mim][TfO], trimethylpropylammonium bis(trifluoromethanesulfonyl)amide ([$N_{1,1,1,3}$][TFSA], Kanto Chemical), and 1-butyl-3-methylimidazolium bis(trifluoromethanesulfonyl)amide ([C_4mim][TFSA], Kanto Chemical). [$N_{1,1,1,3}$][TFSA] and [C_4mim][TFSA] were dried at 343 K under vacuum prior to use. In the next procedure, the resulting Pt-NP-dispersed IL and 3 mg of SWCNT (diameter 1–3 nm, EC 1.5-P, Meijo Carbon) or MWCNT (>90% carbon basis, diameter 2–6 nm, Aldrich) were mixed thoroughly by grinding them together with an agate mortar at room temperature for 30 min. The mixture was then ultrasonically washed with 2-propanol, centrifuged three times, and subsequently dried at 333 K under vacuum for 2 h. A commercially available Pt NPs-supported carbon catalyst (Pt–C) (TEC10V30E, Tanaka Kikinzoku Kogyo K.K.) with 28.9% Pt loading was used for comparison.

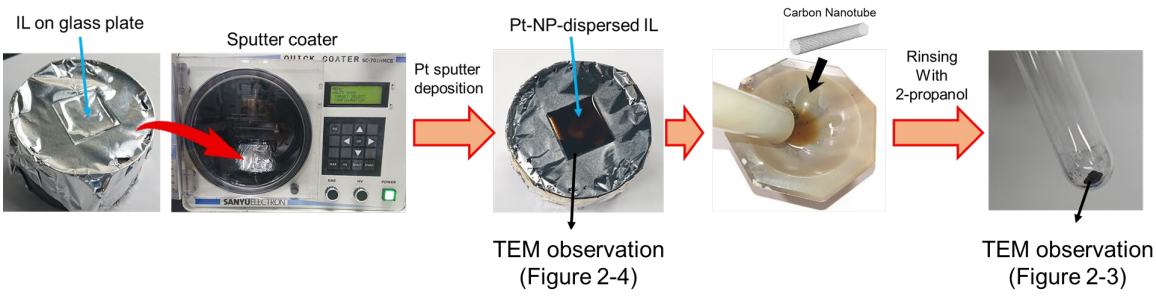

Figure 2-2. The procedure for the preparation of Pt-NP-supported CNT electrocatalysts

2-2-3. Characterization

The zeta potentials of the SWCNT and IL-modified SWCNTs were measured using a Malvern Zetasizer Nano-ZS system. The SWCNT surfaces were modified with IL using the

same grinding method as that for the adsorption of the Pt NPs on the SWCNT (the latter procedure is shown in Figure 2-2), except that Pt-NP-free IL was used. The resultant IL-modified SWCNT powder was ultrasonically dispersed in 2-propanol for 30 min before the zeta potential measurements. The Pt content of the Pt-NP-supported carbon materials was estimated using an inductively coupled plasma atomic emission spectrometer (ICP-AES, Shimadzu ICPS-7510). The specimens for the ICP-AES measurements were prepared by dissolving the Pt NPs adsorbed onto the carbon support in hot aqua regia. Transmission electron microscopy (TEM) of the Pt-NP–carbon materials was conducted using Hitachi H-7650 at an acceleration voltage of 100 kV. Image processing software (Image J) was employed to analyze the TEM images to obtain the size distribution of the Pt NPs. Scanning electron microscope (SEM) observation was carried out using Hitachi SU-5000. X-ray photoelectron spectroscopy (XPS) was conducted using a Shimadzu KRATOS AXIS-165x system equipped with an aluminum target. Raman spectra of the samples were collected by Nanophoton RAMANview using a 532 nm laser source.

2-2-4. Electrochemical analysis

A glassy carbon (GC) rotating disk electrode (RDE; surface area = 0.196 cm^2) connected to a Pine Instruments AFMSRCE electrode rotator was used as the working electrode. The surface of the GC-RDE was polished to a mirror finish with a slurry of 0.06 μm alumina and then rinsed with Milli-Q water and acetone prior to use. To immobilize the carbon-supported Pt NPs on the GC-RDE surface, the carbon material inks were prepared by ultrasonically dispersing the carbon-supported Pt NPs in a mixture of 2-propanol and water (3:1, w:w) for 30 min. Subsequently, a certain amount of the ink was spread onto the GC disk at a loading of 7.5 μg_{Pt} cm^{-2} and slowly dried under saturated 2-propanol vapor. Then, a very thin Nafion® film was coated on the dried layer by placing 5 μL of 0.1 wt% Nafion solution on the dried layer and

drying it. Electrochemical measurements were conducted in a three-electrode glass cell with a GC-RDE working electrode, a Pt mesh counter electrode, and a reversible hydrogen electrode (RHE) connected to the cell by a Luggin capillary as the reference electrode. The specimen on the working electrode was electrochemically cleaned by 100 cycles of potential scanning between 0.05–1.20 V at 50 mV s^{-1} under N_2 atmosphere prior to use. To investigate the direct electronic interaction between the Pt NPs and CNTs in the composites, CO stripping measurement was conducted after CO was electrochemically adsorbed onto Pt NPs by the potentiostatic method at 0.10 V while bubbling CO gas into 0.5 M aqueous H_2SO_4 solution for 10 min. Using the CO-adsorbed carbon-supported Pt NPs electrode, multiple cyclic voltammetry was conducted between 0.05 and 1.2 V (*vs*. RHE) at a scan rate of 5 mV s^{-1}. For this analysis, the electrolyte was pretreated by bubbling N_2 gas for 20 min to remove the residual free CO gas.

2-3. Results and discussion

2-3-1. Zeta potential measurements of SWCNT and IL-modified SWCNT

As mentioned in the introductory remarks, we have developed a method to prepare Pt–carbon catalysts in which the carbon support material and the Pt-NP-dispersed IL prepared using the IL-sputtering method are thoroughly mixed and then heated at 573 K. This method is capable of immobilizing Pt NPs on any kind of carbon material, but the selection of the IL is essential. For example, ammonium cation-based ILs enable Pt NPs to stick to carbon surfaces, whereas imidazolium cation-based ILs do not.[70, 71] If the hetero-aggregation induced by the electrostatic attraction is the main cause of the spontaneous adsorption of the Pt NPs onto the carbon support material, it is necessary to measure the charge state of the materials, that is, the type and quantity of the charges. Although the inability to separate Pt NPs from IL makes it impossible to probe the charge state of the nanoparticles, they can be considered negatively

charged in the ILs that we have employed to date because these ILs possess sulfate or sulfonic anions, which are well known to possess a specific ability to adsorb onto the Pt surface.[43, 103] Therefore, the surface charge states of the SWCNT and IL-modified SWCNT were investigated using the zeta potential measurement. The data obtained are shown in Table 2-1.

Table 2-1. Zeta potentials of IL-coated SWCNTs in *i*-propanol

Ionic liquids	Zeta potential / mV
–*	−2.64
$[N_{1,1,1,3}][TFSA]$	−0.031
$[C_4mim][TFSA]$	−0.22
$[C_4mim][TfO]$	0.86
$[dema]HSO_4$	18.7
[dema][TFSA]	11.7
[dema][TfO]	23.9

*: pristine SWCNT.

The pristine SWCNT presented a slightly negative potential (−2.6 mV). This is probably due to the carbonyl and/or carboxyl groups that may be generated at the ends of tubes where the sp^2 structures are cut. Modification of the SWCNT with $[N_{1,1,1,3}][TFSA]$, $[C_4mim][TFSA]$, and $[C_4mim][TfO]$ caused positive shifts in the zeta potential, but the shift differences were quite small, contrary to our expectations. In fact, the order of the positive shift differences gave no explanation as to why the experimental results with $[N_{1,1,1,3}][TFSA]$ worked well for Pt-NP

adsorption using the IL-sputtering method whereas other ILs did not. It is probable that the heating process after the grinding of the mixture causes some structural and/or chemical alterations, providing the atmosphere that induces the spontaneous adsorption of Pt NPs onto the carbon support. This conjecture has become our research subject that will be addressed.

We started to develop the IL-sputtering method with neutral ammonium-based ILs such as $[N_{1,1,1,3}][TFSA]$ and $[N_{1,4,4,4}][TFSA]$. Subsequently, when an attempt was made to add electropolymerizable compounds to the IL, with the aim of improving the electrical conductivity between the Pt NPs and the carbon support, a protic IL, $[DEMA][HSO_4]$, was selected by taking into account the solubility of the additives and the chemical condition for their electropolymerization.[72, 73] The zeta potential measurements conducted in the present study revealed that three kinds of protic [dema]-based IL brought about a large positive shift when they were used as SWCNT-modifying agents, indicating that the SWCNT had sufficient positive charges.

As heating was the requisite process to induce Pt-NP adsorption using neutral ILs as a medium, this process was conducted after mixing the Pt-NP-dispersed protic IL and the carbon material as a matter of course. However, zeta potential measurements predicted the possibility that Pt-NP adsorption onto the SWCNT takes place spontaneously without the heating process. With that expectation in mind, using six kinds of IL, the mixing of the SWCNT and the Pt-NP-dispersed IL was conducted for 30 min at room temperature, followed by rinsing with 2-propanol and drying. Figure 2-3 shows TEM images of the resultant specimens. Similar to the results that we have obtained so far, Pt NPs were hardly observed on the samples prepared at room temperature using $[N_{1,1,1,3}][TFSA]$, $[C_4mim][TFSA]$, and $[C_4mim][TfO]$ (Figures 2-3a–c). However, the immobilization of the Pt NPs on the SWCNT was clearly observed in the specimens prepared from the mixtures of the SWCNT and the Pt-NP-dispersed [dema]-based ILs (Figures 2-3d–f). Pt-NP adsorption was also achieved for the sample prepared by mixing

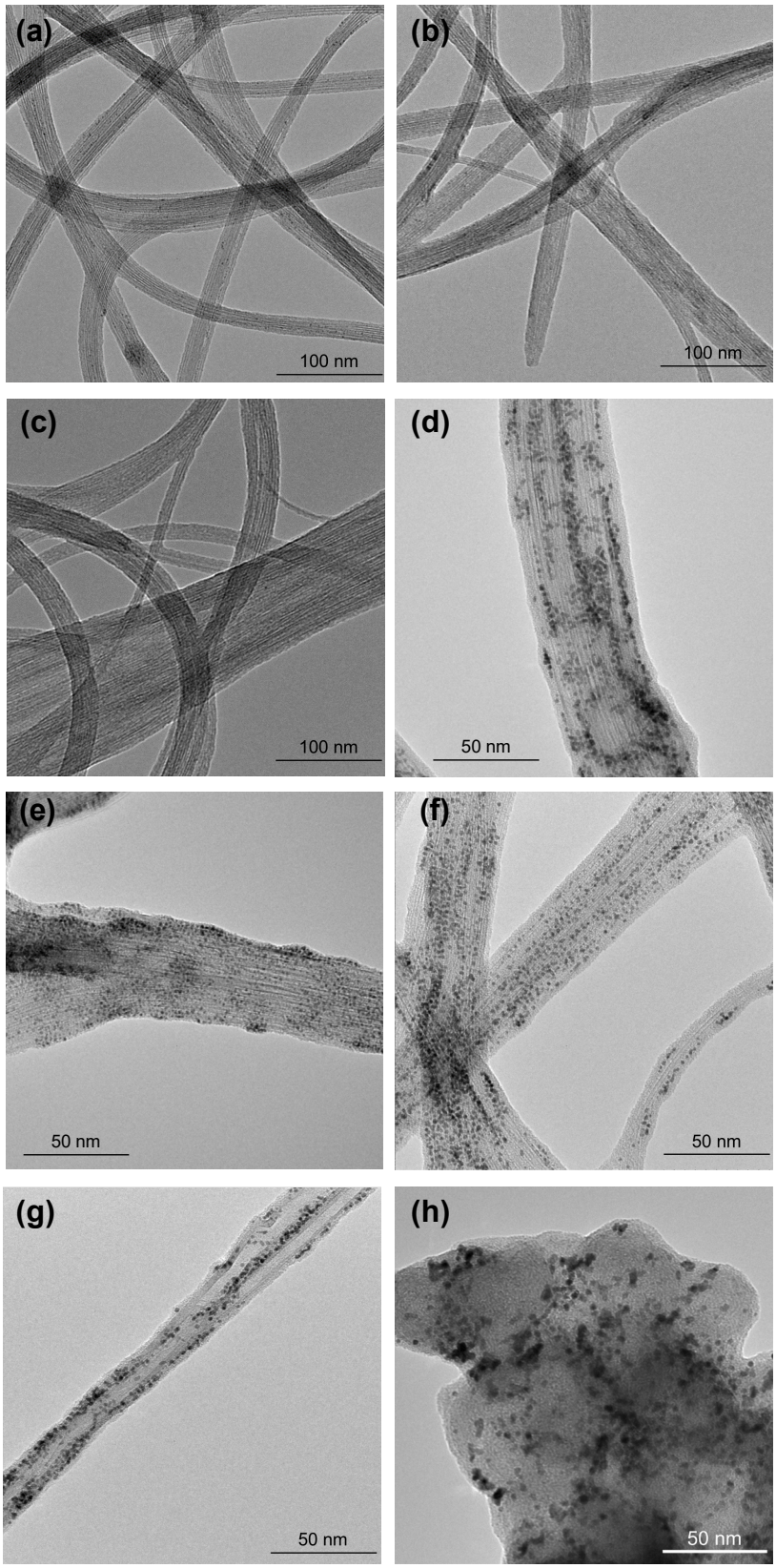

Figure 2-3. TEM images of Pt-NP-supported SWCNTs prepared with different ILs: (a) $[N_{1,1,1,3}][TFSA]$; (b) $[C_4mim][TFSA]$; (c) $[C_4mim][TfO]$; (d) $[dema]HSO_4$; (e) [dema][TFSA]; (f) [dema][TfO] and of (g) Pt-NP-supported MWCNT prepared with [dema][TfO] and (h) commercially available Pt-C.

the MWCNT with the Pt-NP-dispersed [dema][TfO] (Figure 2-3g). These results strongly support our assumption that the electrostatic interaction between the negatively charged Pt NPs and the positively charged IL-modified SWCNT is the main driving force behind the spontaneous adsorption of the Pt NPs onto the SWCNT. Furthermore, it is possible that a protic moiety contained only in protic cations, such as $[dema]^+$, anchored the adsorbed Pt NPs through the formation of a Pt–H–N bond.[104]

2-3-2. Characterization of Pt–CNTs

Figure 2-4 shows TEM images with particle-size distributions of Pt NPs prepared by the IL-sputtering method using six kinds of IL. The particle-size distributions of the Pt NPs immobilized on the SWCNT and MWCNT with three protic [dema]-based ILs were estimated from the TEM images (Figures 2-3d–g), and the histograms obtained are shown in Figure 2-5, which also shows that of the commercial Pt–C. By comparing Figure 2-5 with Figure 2-4, it can be seen that Pt-NP adsorption did not result in any significant change in particle size and that the mean Pt-particle size and size distribution of the prepared Pt-SWCNT were, respectively, smaller and narrower than those of the commercial Pt–C catalyst (Figure 2-5e). In this study, we focused on a Pt-SWCNT and Pt-MWCNT prepared using [dema][TfO] as a medium because both samples exhibited higher Pt-NP dispersibility than Pt-CNTs prepared

Table 2-2. Loading amount and particle size of CNT-supported Pt NPs

	Loading amount of Pt NPs / wt%	Particle size / nm	
		Initial	After ADT
Pt-SWCNT	23.6	1.9±0.4	2.6±0.8 / 6.9±3.6*
Pt-MWCNT	29.2	1.9±0.3	4.2±0.9
Pt-C	28.9	3.7±0.7	5.0±1.4

using other [dema]-based ILs. The Pt-loading amounts of the Pt-SWCNT and Pt-MWCNT

were 23.6 and 29.2 wt%, respectively, which were comparable to that of the Pt–C catalyst (28.9 wt%). The Pt-NP particle size and loading amount are summarized in Table 2-2. The Pt-SWCNT and Pt-MWCNT SEM images and the energy dispersive X-ray spectroscopy (EDX)

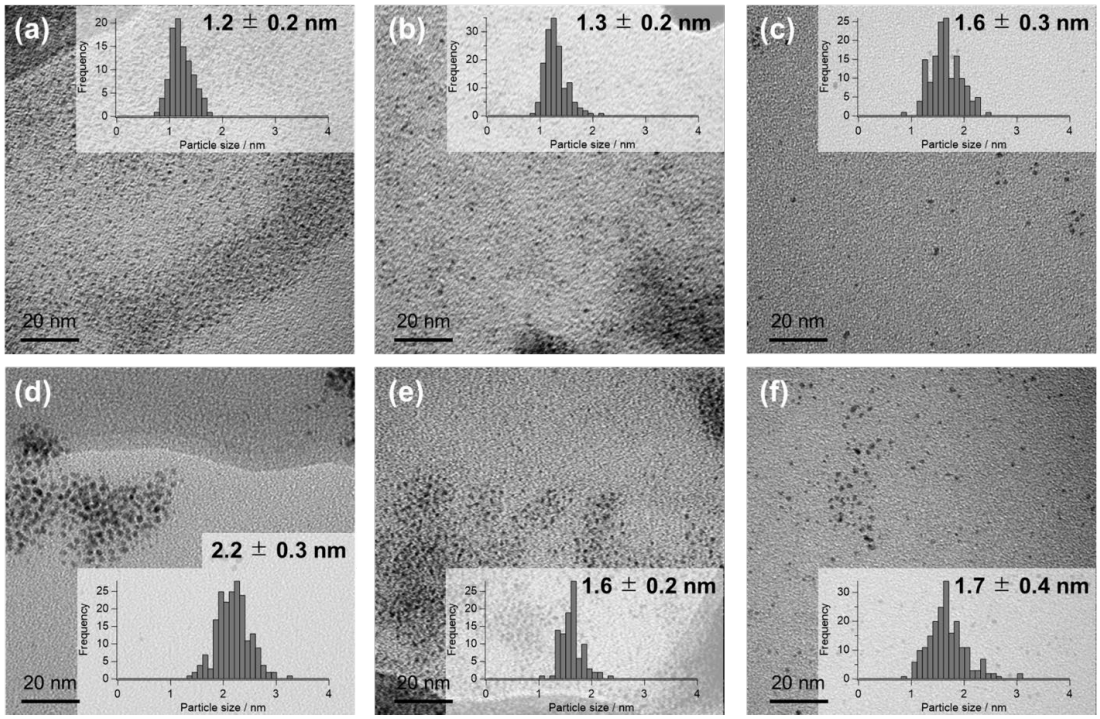

Figure 2-4. TEM images with particle size distribution of Pt NPs prepared by Pt-sputtering onto different ILs; (a) $[N_{1,1,1,3}][TFSA]$, (b) $[C_4mim][TFSA]$, (c) $[C_4mim][TfO]$, (d) $[dema]HSO_4$, (e) [dema][TFSA], and (f) [dema][TfO].

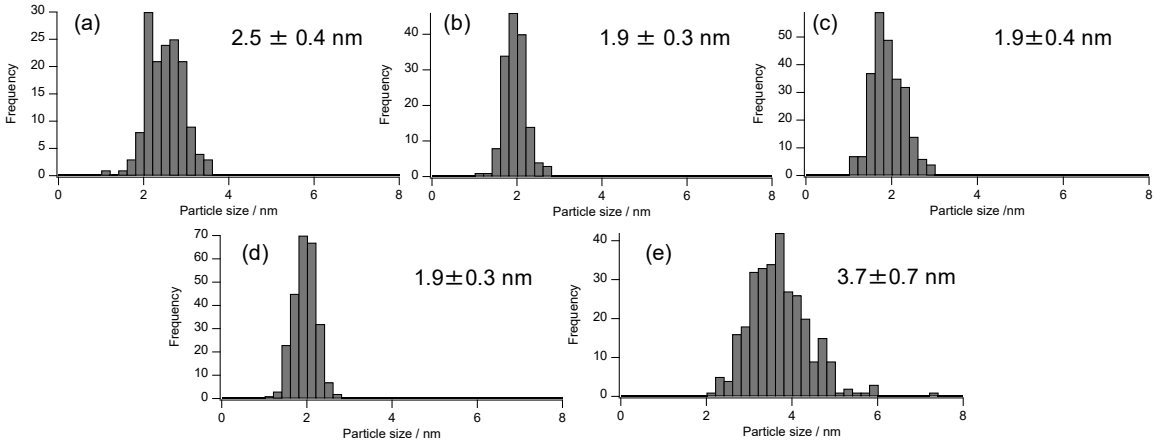

Figure 2-5. The particle size distributions of Pt-SWCNT prepared using (a) $[dema]HSO_4$, (b) [dema][TFSA] and (c) [dema][TfO] and those of (d) Pt-MWCNT and (e) commercial Pt–C.

spectra and mapping images for Pt and C are shown in Figure 2-6. The EDX spectra of both species show not only peaks due to Pt and C but also weak peaks due to N, S, and F atoms, indicating the existence of an IL residue, as expected. Unfortunately, the Pt NPs were too small to be observed with our FE-SEM instrument, but the EDX-mapping images distinctly revealed that they were distributed on each CNT.

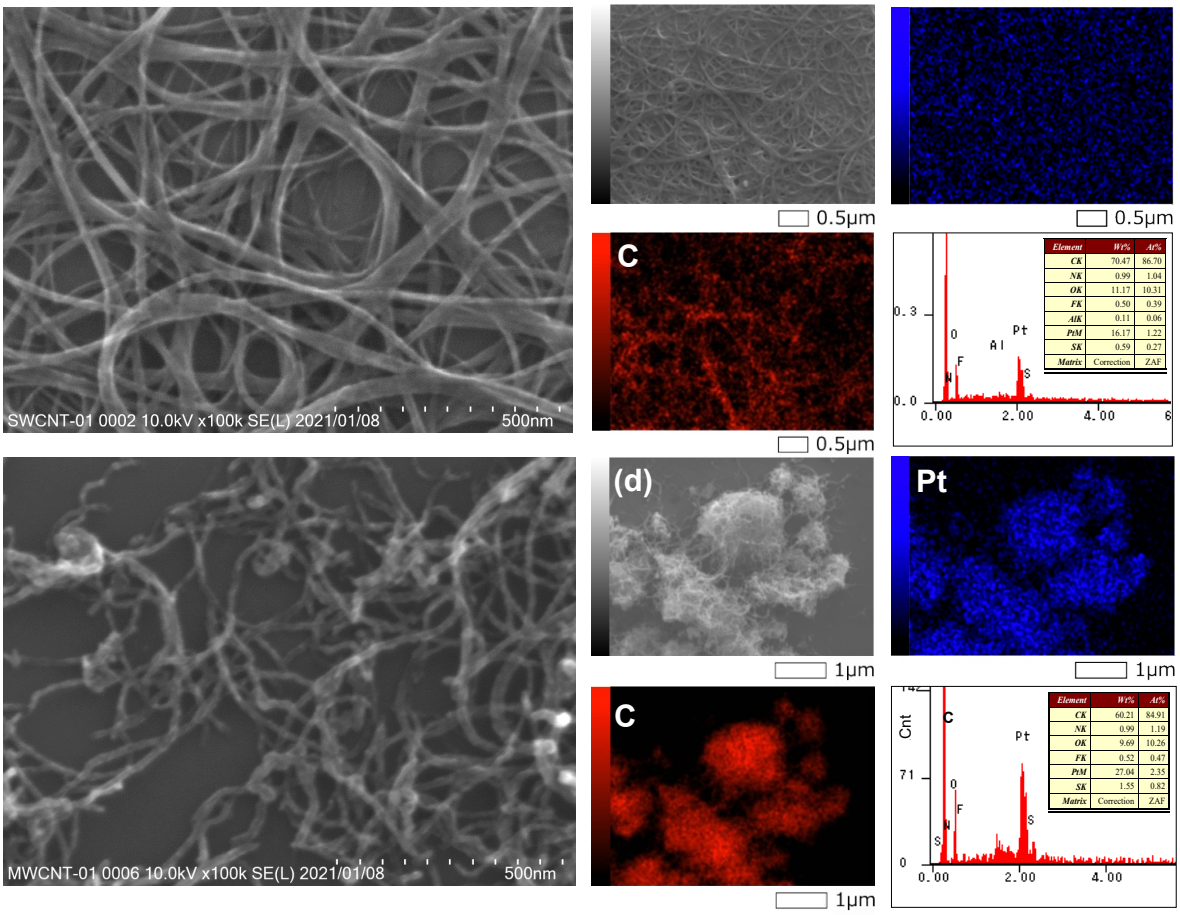

Figure 2-6. SEM images and SEM-EDX spectra and mapping images for Pt and C of (a,b) Pt-SWCNT and those of (c,d) Pt-MWCNT.

The electrochemical CO-stripping measurement was conducted for the prepared Pt-CNT and the commercial Pt–C. The CVs obtained at 5 mV s^{-1} in H_2SO_4 solution are shown in Figure 2-7. The peak potential values were 0.79, 0.77, and 0.76 V, and the full width at half maximum (FWHM) values were 33, 45, and 51 mV for the Pt-SWCNT, Pt-MWCNT, and Pt–C, respectively. As for Pt NPs smaller than 5 nm, the peak potential of CO-stripping is known to depend to some extent on the size of the Pt NPs; the smaller the particle size is, the more positive is the peak potential shift.[105-107] This dependence property, of course, produces another dependency, which is an increase in the FWHM with a decrease in particle-size uniformity. On this basis, the electrochemical CO-stripping results (Figure 2-7) roughly reflect the results shown in Figure S3. Another major cause of the potential shift is the electronic interaction between the Pt NPs and the carbon support. Alonso-Vante et al. investigated the effects of this interaction using MWCNTs and Vulcan XC-72 carbon supports onto which Pt NPs were directly deposited by chemical means.[108-110] They demonstrated that the peak potential of CO-stripping from Pt NPs on an sp^2-carbon surface was negatively shifted by approximately 0.1 V compared to that from Pt NPs on an sp^3-carbon surface, resulting in the splitting of the oxidation peak into two at 0.68 V vs. RHE (peak I) and 0.76 V vs. RHE (peak II) when a CO-stripping CV was obtained by the Pt NPs deposited on MWCNTs that possessed both sp^2 and sp^3 domains. The theoretical calculations of the electron interaction between CO, Pt, and the carbon support predicted the enhancement of the electron density of Pt on an sp^2-carbon surface that increased the catalytic oxidation of CO by the Pt NPs deposited on the MWCNT. By contrast, the electronic interaction between CO and Pt did not differ regardless of whether the carbon support had an sp^3 surface.

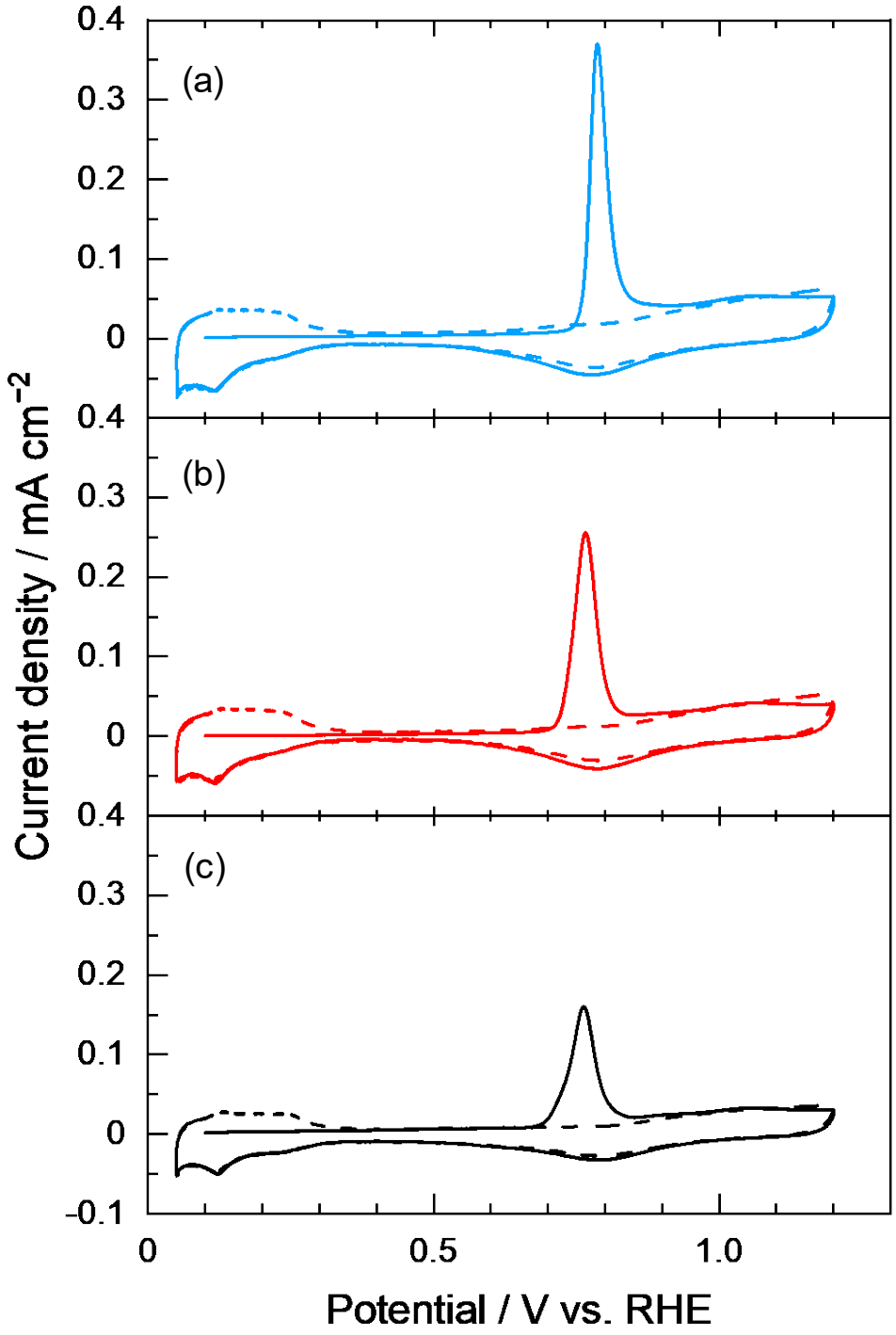

Figure 2-7. CO-stripping CVs of (a) Pt-SWCNT, (b) Pt-MWCNT, and (c) commercial Pt-C obtained in 0.5 M H_2SO_4 at 5 mV s^{-1}; (——) first cycle; (- - -) second cycle.

Figure 2-8 shows the Raman spectra of the SWCNT and MWCNT before and after Pt-NP adsorption. Both the pristine SWCNT and the Pt-SWCNT showed a strong peak at about 1,580 cm^{-1} and an additional weak peak at about 1,350 cm^{-1}, which were attributed to the G and D

bands, respectively. Moreover, the G band can be deconvoluted into G^+ and G^- bands because of the degeneracy of the G band.[111] In the Raman spectra of the pristine MWCNT and the Pt-MWCNT, both G and D bands appeared distinctly with comparable intensities. The G band is the characteristic band due to the in-plane vibration of the sp^2 carbons, whereas the D band corresponds to the disorder-induced band in the defective graphite structure.[112] If the Pt-SWCNT and the Pt-MWCNT that we prepared provided direct contact between the Pt NPs and CNTs, it was expected that the Pt-SWCNT showed peak I dominantly and the Pt-MWCNT showed peaks I and II. Accordingly, the CV results shown in Figure 2-7, in which all catalysts show only peak II contrary to expectations, supported experimentally our previous assumption that a trace amount of IL working as an adhesive bond hinders direct electronic interaction between the Pt NPs and the carbon support. The lack of difference in the Raman peak-intensity ratio of the D band to G band (I_D/I_G) between the SWCNT and the Pt-SWCNT also revealed that there was no chemical bonding formation between the Pt NPs and the sp^2 surfaces.[113]

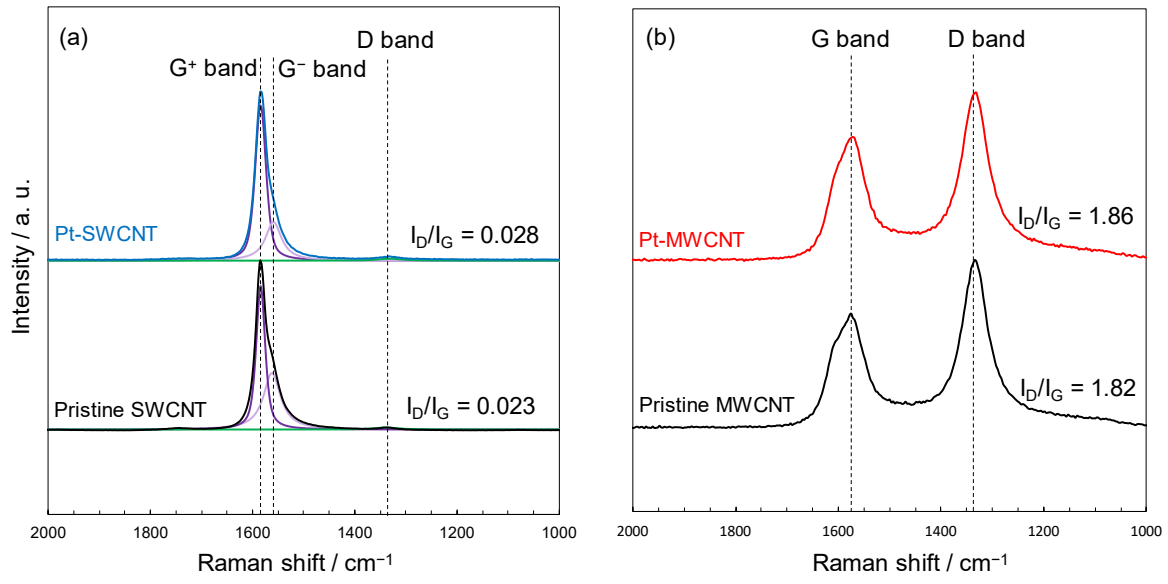

Figure 2-8. Raman spectra of (a) pristine SWCNT (black), Pt-SWCNT (blue), (b) pristine MWCNT (black), and Pt-MWCNT (red).

XPS measurements were conducted to investigate the electronic structure and electronic state density of the Pt NPs on the carbon supports. The obtained spectra for the Pt-4f core level are shown in Figure 2-9. Although the XPS spectra were characterized by three different electronic states, Pt^0, Pt^{2+}, and Pt^{4+}, the major electronic state was Pt^0 in all cases. Binding energy is known to be affected by the electron density of the material as an increment in electron density shifts the binding energy toward a lower energy. In the above-mentioned case of Pt NPs directly deposited onto a carbon support, the Pt^0-$4f_{7/2}$ signal of the Pt NPs deposited onto the MWCNT showed a downshift of 210 meV compared with that deposited onto the Vulcan.[109] The electron transfer causing this energy density change is the reason for the negative shift in the oxidation peak of the CO-stripping as mentioned above. On the contrary, the Pt-SWCNT and Pt-MWCNT, which showed no peak I in their CO-stripping CV (Figure 2-7), did not exhibit any downshift in the Pt^0-$4f_{7/2}$ signal in comparison with the commercial Pt–C. Rather, the Pt^0-$4f_{7/2}$ signal position of the Pt-SWCNT (71.79 eV) and Pt-MWCNT (71.78 eV) was apparently higher than that of the commercial Pt–C (71.55 eV). This fact provides further evidence that there was no electronic interaction between the Pt NPs and the carbon support because of the presence of a trace amount of IL. Another factor that affects the binding energy is the particle size; a decrease in particle size causes a peak shift upward.[114, 115] This effect should account for the binding energy shift that we obtained because the particle size of the commercial Pt–C was apparently larger than that of the Pt-SWCNT and Pt-MWCNT, as shown in Figure 2-5.

Figure 2-10 shows the CVs recorded for the stationary Pt-SWCNT, Pt-MWCNT, and commercial Pt–C in an N_2-saturated 0.1 M $HClO_4$ solution. Redox waves corresponding to hydrogen adsorption/desorption and Pt oxidation/reduction characteristic of platinum were observed. The ECSA of Pt was estimated by an integration of reduction currents caused by hydrogen adsorption on the basis of the electric charges consumed by the hydrogen

adsorption/desorption on the Pt (210 μC cm_{Pt}^{-2}). The ECSAs estimated from the CVs are shown in Table 3. The ECSA data exhibited good agreement with the Pt surfaces estimated from the CO-stripping measurements. The Pt-SWCNT and Pt-MWCNT ECSAs were much

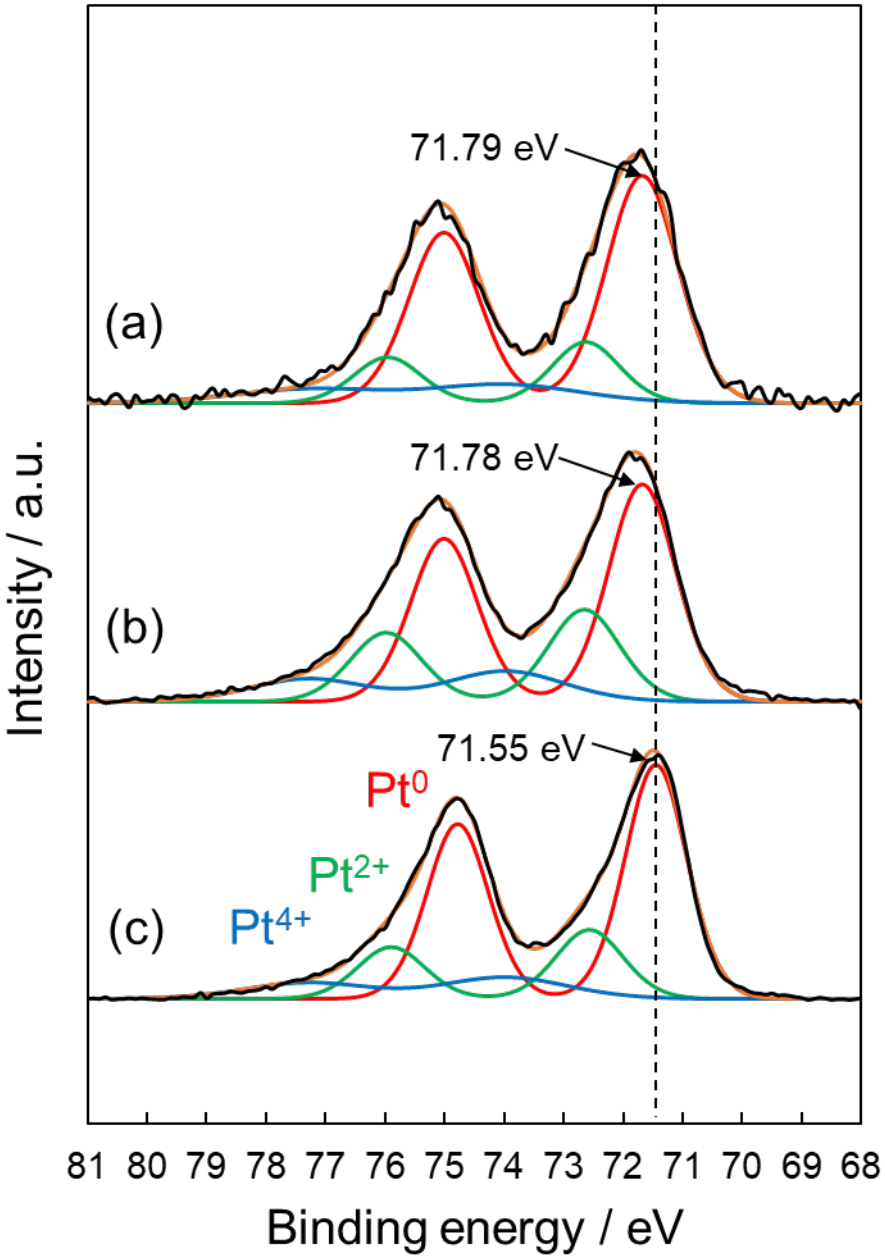

Figure 2-9. XPS spectra of the Pt-4f core level of (a) Pt-SWCNT, (b) Pt-MWCNT, and (c) commercial Pt-C. Red, green, and blue lines in the Pt-4f spectra correspond to the Pt^0, Pt^{2+}, and Pt^{4+} signals, respectively.

larger than that of the Pt–C owing to their smaller Pt-NP size. However, the result showing that the Pt-MWCNT had a smaller ECSA than the Pt-SWCNT contradicted the result demonstrating the similar mean size of their Pt NPs. This could be attributed to the higher dispersion of the Pt NPs on the SWCNT, identified by closely observing the TEM images (Figures 2-3f and g) in which flocculation of some Pt NPs can be seen for the Pt-MWCNT, wheras it is hard to find such configuration for the Pt-SWCNT. It is probable that the Pt NPs that touched each other decreased their surface areas estimated by electrochemical means.

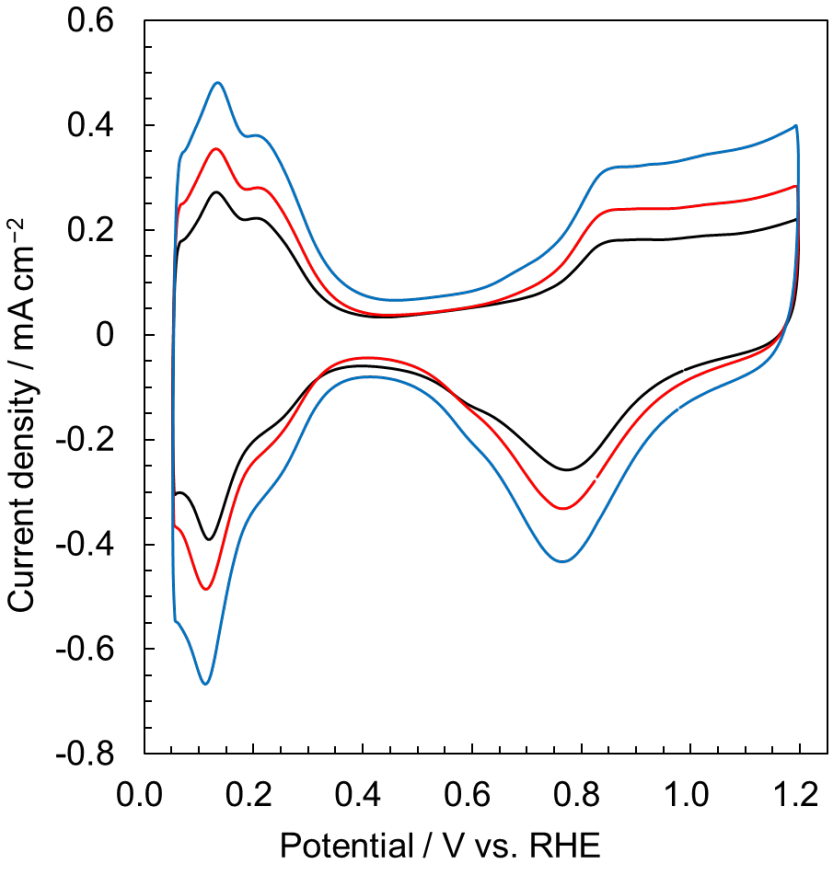

Figure 2-10. CVs of Pt-SWCNT (blue), Pt-MWCNT (red), and commercial Pt-C (black) taken in N_2-saturated 0.1 M $HClO_4$ at a sweep rate of 50 mV s^{-1}.

2-4. Conclusions

In conclusion, the adsorption of Pt NPs onto CNT was caused by electrostatic force between negative-charge Pt NPs by adsorption of anion and positive-charged CNT by adsorption of cation. Especially, [dema]-based protic IL made a surface of CNT positive-charged more than +10 mV and Pt NPs dispersed in [dema]-based protic IL spontaneously adsorbed onto CNT even at room temperature. The spontaneous adsorption of Pt nanoparticles onto carbon nanotubes during the mixing procedure occurred as a result of the electrostatic attraction between negatively charged Pt NPs by anion adsorption and positively charged CNTs by cation adsorption. The ability to skip the heating step when using protic IL is undoubtedly advantageous because Pt NPs, which exhibit high catalytic activity due to their narrow size distribution, can be adsorbed onto the carbon support without changing size. The Pt NPs were immobilized on the CNTs by noncovalent bonding between Pt and CNTs, with protic IL acting as a nanoglue.

Chapter 3

ORR Activity of CNT-supported Pt NPs Prepared at Room Temperature

3-1. Introduction

Generally, Pt-based electrocatalysts are used to accelerate the ORR of PEMFCs. However, the high cost of Pt-based electrocatalysts has limited its further application in PEMFCs. To overcome this limitation, several researchers have devoted tremendous efforts to reduce Pt usage in PEMFCs. Various promising approaches have been introduced to this end, including the utilization of Pt–transition metal alloy nanoparticles (NPs),[116-118] Pt-based core–shell NPs,[119-121] and shape-controlled Pt and its alloy-based nanomaterials.[78, 79, 122-124] On the other hand, it is also important to improve the durability of electrocatalysts to maintain a high catalytic activity over the lifetime of devices.[81, 82] Typically, there are two main deterioration mechanisms for ORR electrocatalysts; (i) the detachment of Pt NPs from carbon supports due to the corrosion caused by an electrochemical oxidation that is triggered by starting and stopping devices,[125, 126] (ii) the growth of Pt NPs during operation due to the migration of atoms and/or the fusion of NPs.[127-129] The use of highly crystalline sp^2 carbon materials as a carbon support for ORR electrocatalysts has been considered as an effective method to impede the carbon corrosion reaction.[130, 131] The former is enhanced when carbon supports with many defects were used, whereas the latter is caused by a weak Pt–carbon interaction.[132-134] However, the defect-free surface and strong interaction with Pt NPs are contradictive demands for carbon supports because Pt NPs bind more strongly to the functional groups of carbon, i.e., carboxyl and quinone groups. Therefore, researchers are finding an optimal point to balance these two contradicting effects.[133]

In Chapter 2, it was described that Pt NPs dispersed in [dema][TfO] prepared by ionic liquid-sputtering method were homogeneously immobilized on pristine CNT by only agitation at room temperature. This method is extremely simple among preparation method of CNT-supported Pt NPs. This chapter describes ORR activity and durability of the obtained Pt-CNT. The Pt-SWCNT and Pt-MWCNT composites exhibited higher ORR catalytic activity and durability than Pt-C. Furthermore, after the accelerated deterioration test (ADT), the aggregation behavior of Pt NPs on Pt-SWCNT was significantly different than that of Pt NPs on Pt-MWCNT and Pt-C. This is because Pt nanorods were formed in the channels of the SWCNT bundles, which are known to exhibit high catalytic activity for ORR, during the ADT. As described above, when Pt NPs are supported on highly crystalline carbon, particle growth is easy to occur due to weak Pt-carbon interaction although highly crystalline carbon support shows high durability against carbon corrosion reaction. However, in this study, controlling a direction of migration maintained ORR activity and this electrocatalyst had both highly crystalline of carbon support and durability against particle growth during an operation of fuel cell. These findings will provide insights for the development of functional ORR electrocatalysts in the future.

3-2. Experimental section

3-2-1. Electrochemical analysis

Cyclic voltammograms (CVs) and linear sweep voltammograms (LSVs) were obtained using a computer-controlled Hokuto Denko HZ-5000 potentiostat/galvanostat. The specimen on the working electrode was electrochemically cleaned by 100 cycles of potential scanning between 0.05–1.20 V at 50 mV s^{-1} under N_2 atmosphere prior to use. The electrochemical surface area (ECSA) of Pt NPs on the specimens was estimated from hydrogen desorption coulombic charge in the cyclic voltammogram under a N_2 atmosphere after subtracting the

double layer charging current from the original voltammogram.

The RDE-LSVs for the ORR were obtained from the rotating GC-RDE with the Pt–carbon at 1,600 rpm in an O_2-saturated 0.1 M $HClO_4$ solution. The electrocatalytic activity was evaluated on the basis of the kinetic current (I_k) estimated by[135]

$$I_k(A) = \frac{I_{lim}(A) \times I_E(A)}{\left(I_{lim}(A) - I_E(A)\right)} \quad (1)$$

where I_{lim} (A) is the measured limiting current and I_E (A) is a current value at the potential of E. Mass activity was calculated by dividing I_k by the amount of Pt loading on the disk electrode. The durability of the Pt–carbon catalyst was examined using the load-cycle test, which is one of the ADTs proposed by the Fuel Cell Commercialization Conference of Japan.[136] A continuous square-wave potential variation of 0.6 V for 3 s and 1.0 V for 3 s was applied to the electrode in an N_2-saturated 0.1 M $HClO_4$ aqueous solution at room temperature. The catalytic activities of the Pt–carbon catalysts subjected to 20,000 cycles of the ADT were evaluated after sufficiently bubbling O_2 in the electrolyte solution.

3-3. Results and discussion

3-3-1. Electrocatalytic activities of CNT-supported Pt NPs

The RDE-LSVs given by the three catalyst-coated electrodes in O_2-saturated 0.1 M $HClO_4$ solution are shown in Figure 3-1a, and the kinetic current (I_k) density values estimated from the obtained RDE-LSVs were plotted as a function of potential to evaluate their Tafel slopes, as shown in Figure 3-1b. The RDE-LSV curves obtained for the Pt-SWCNT and Pt-MWCNT were mostly coincident, and the half-wave potential definitely shifted toward the positive, compared to that of the commercial Pt–C, by 38 mV, exhibiting the higher electrocatalytic activities of the Pt-CNTs prepared in this study. Although such potential differences were also apparent in the Tafel plots, all plots gave a slope of 60 mV dec^{-1} in the low current-density

region and a slope of 120 mV dec^{-1} in the high current-density region as many other studies have reported.[78, 79, 137] As mentioned previously, we assume that a trace amount of IL remains on the catalysts prepared by the IL-sputtering method, which works as an adhesive bond for the adsorption of Pt NPs onto a carbon support. This assumption does not rule out the possibility that the IL is also attached to the surfaces of the Pt NPs. Even if this assumption is correct, the Tafel plots obtained by the catalysts that we prepared proved that the IL did not significantly affect the catalytic activity toward an ORR as well as its reaction mechanism when the reductive adsorption of O_2, electron transition, and reductive desorption steps were included. The slopes of all plots deviated to values greater than 120 mV dec^{-1} when the current-density became much larger because of the mass transfer limitation. As the Pt-SWCNT demonstrated a deviation at the most positive potential (0.835 V vs. RHE) of the catalysts used, a comparison of I_k at an even more positive potential was indispensable for comparing catalytic activities between different catalysts.[138]

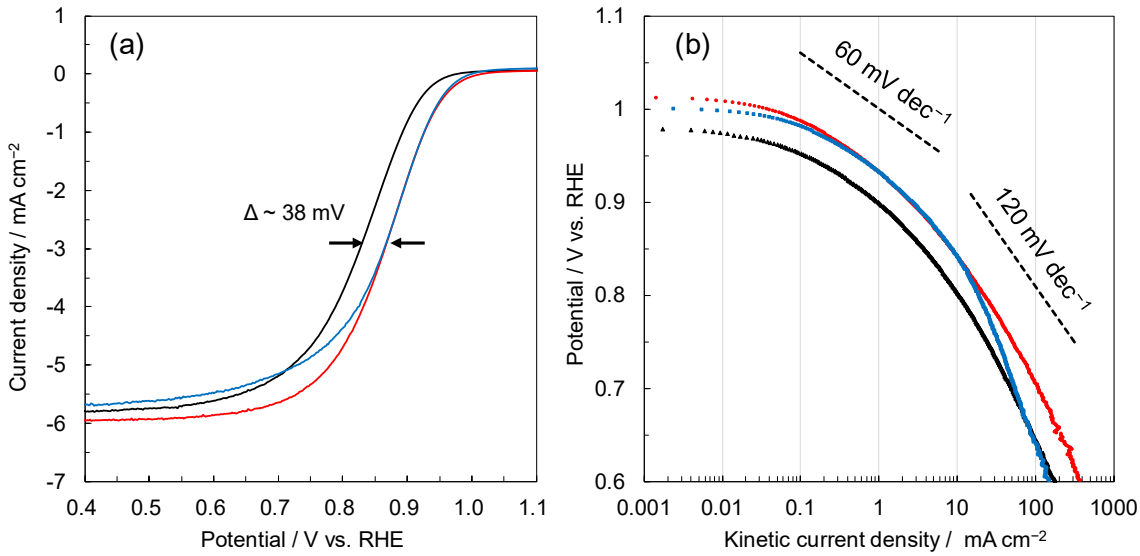

Figure 3-1. (a) RDE-LSVs of Pt-SWCNT (blue), Pt-MWCNT (red), and commercial Pt-C (black) obtained in O_2-saturated 0.1 M $HClO_4$ at 10 mV s^{-1} with a rotation speed of 1,600 rpm; (b) Tafel plots obtained by replotting the RDE-LSVs.

Table 3-1. ECSA, mass activity, and specific activity of electrocatalysts before/after ADT

	ECSA		Mass activity at 0.9 V vs. RHE		Specific activity at 0.9 V vs. RHE	
	Initial /$m_{Pt}^2\ g_{Pt}^{-1}$	After ADT /$m_{Pt}^2\ g_{Pt}^{-1}$	Initial /A g_{Pt}^{-1}	After ADT /A g_{Pt}^{-1}	Initial /A m_{Pt}^{-2}	After ADT /A m_{Pt}^{-2}
Pt-SWCNT	100.2	51.4	353.3	374.8	3.52	7.29
Pt-MWCNT	76.2	27.9	347.8	291.6	4.56	10.4
Pt–C	55.5	29.8	132.1	90.3	2.38	3.03

The mass activity and specific activity of the three electrodes toward an ORR estimated from the I_k values at 0.90 V (*vs*. RHE) are summarized in Table 3-1. The mass activities of the Pt-SWCNT and Pt-MWCNT electrodes were approximately 2.5 times higher than that of the Pt–C electrode. The specific activities were also improved compared with those of the Pt–C. We believe that these favorable catalytic activities resulted from the smaller particle size with the narrow size distribution of the Pt NPs prepared by the IL-sputtering method and their high dispersibility on the CNTs having high electrical conductivity.[139, 140] As already explained, the XPS spectra (Figure 2-9) demonstrated an upshift in the Pt-4f binding energy of the Pt-CNTs compared with the commercial Pt–C owing to a smaller particle size. This leads to a decrease in the electron density of the Pt-4f core level that naturally accompanies an increase in the 5d-band vacancy. Both experimental and theoretical studies revealed that such a change in the electronic status of Pt is effective for enhancing catalytic activity toward ORR.[141, 142]

When the Pt-SWCNT was prepared with an ammonium-based IL by the IL-sputtering, mixing, and heating procedures, the mean size of the Pt NPs was larger and the size distribution was wider than that of the original Pt NPs dispersed in the IL. From these results, it is clear that the heating process causes some aggregation of the Pt NPs. In this regard, the Pt-CNT

preparation method developed in this study, which skips the heating process, has the great advantage that the small size and narrow size distribution of the Pt NPs mean that they can be adsorbed onto the SWCNT as they are. This desirable feature is directly linked to the above-mentioned improvement in catalytic activity.

3-3-2. Accelerated deterioration test of CNT-supported Pt NP

The Pt-SWCNT, Pt-MWCNT, and Pt–C electrocatalysts were subjected to ADT by applying square-wave potential cycles between 0.6 and 1.0 V. Figures 3-2a–f show the CVs and the RDE-LSVs obtained by the three catalyst electrodes in N_2- and O_2-saturated 0.1 M $HClO_4$ solution, respectively, before and after the 20,000-cycle ADT. The ORR activities after ADT were estimated from the I_k values at 0.90 V in the RDE-LSVs, and they are summarized in Table 3. As for the mass activities, the value changes are depicted by the bar chart shown in Figure 3-2g. The 20,000-cycle ADT definitely decreased the ECSA of all catalysts, but change in the reduction currents caused by ORR was quite different between the electrodes. With regard to the Pt–C, reduction currents and mass activity were largely reduced. However, it is notable that the ADT resulted in a slight enhancement of the mass activity of the Pt-SWCNT despite the decrease in ECSA. To understand the origin of this contradicting behavior, the three electrocatalysts subjected to the ADTs were observed by TEM. The TEM images are shown in Figures 3-3a–d, and the size histograms of the Pt NPs estimated by analyzing the TEM images are shown in Figures 3-3e,f and 3-4. A comparison of the histograms shown in Figures 3-4a,b and those shown in Figures 2-5d,e found a monotonical increase in the Pt-NP size of the Pt-MWCNT and Pt–C during the ADT. By contrast, surprisingly, the shape of the Pt NPs of the Pt-SWCNT changed dramatically from spherical (Figure 2-3f) to nanorod-like (Figure 3-3a). The TEM image with higher magnification (Figure 3-3d) clearly shows their presence along the grooves formed at the contacts of the carbon nanotubes in the SWCNT bundle. It was

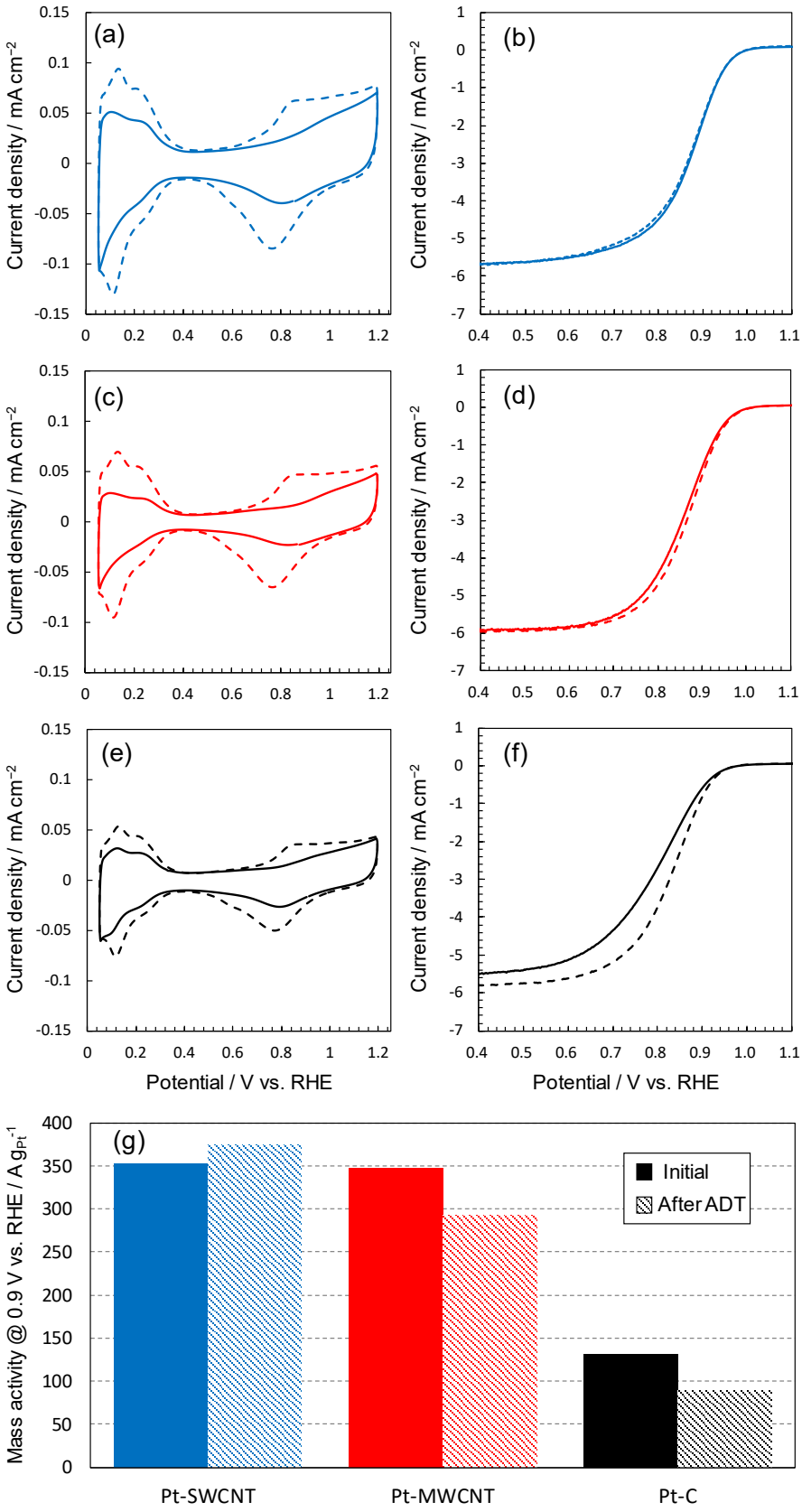

Figure 3-2. CVs and RDE-LSVs of (a,b) Pt-SWCNT, (c,d) Pt-MWCNT, and (e,f) commercial Pt-C before (dashed line, - - -) and after (solid line, ——) 20,000-cycle ADT; (g) comparison of the mass activity estimated from I_k values at 0.90 V vs. RHE.

therefore possible to evaluate the size distribution in the radial and axial directions of the bundle, as shown in Figures 3-3e and 3-3f, respectively. These results provided several hints for considering events during the ADT. The fact that the SWCNT of the Pt-SWCNT, unlike the

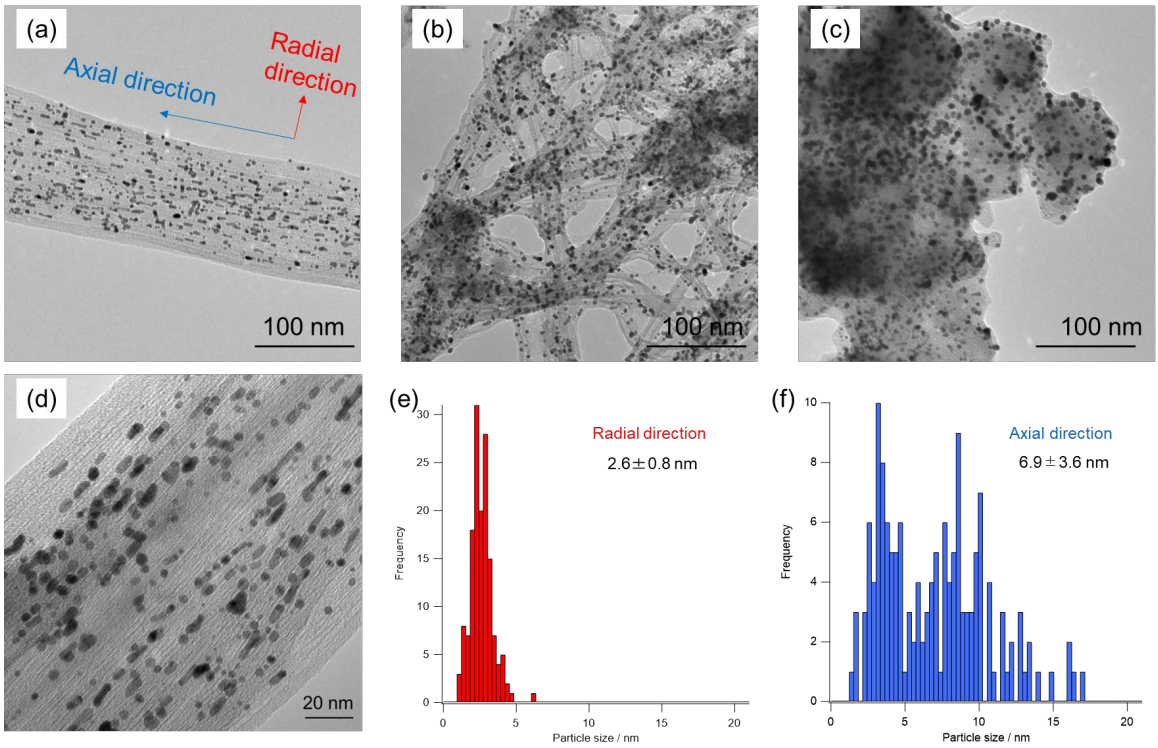

Figure 3-3. TEM images of (a) Pt-SWCNT, (b) Pt-MWCNT, and (c) Pt-C after 20,000-cycle ADT. (d) Enlarged TEM images of the Pt-SWCNT depicted in Figure 6a. Histograms of Pt particle size along the (e) radial and (f) axial direction on the Pt-SWCNT shown in Figure 3-3(a).

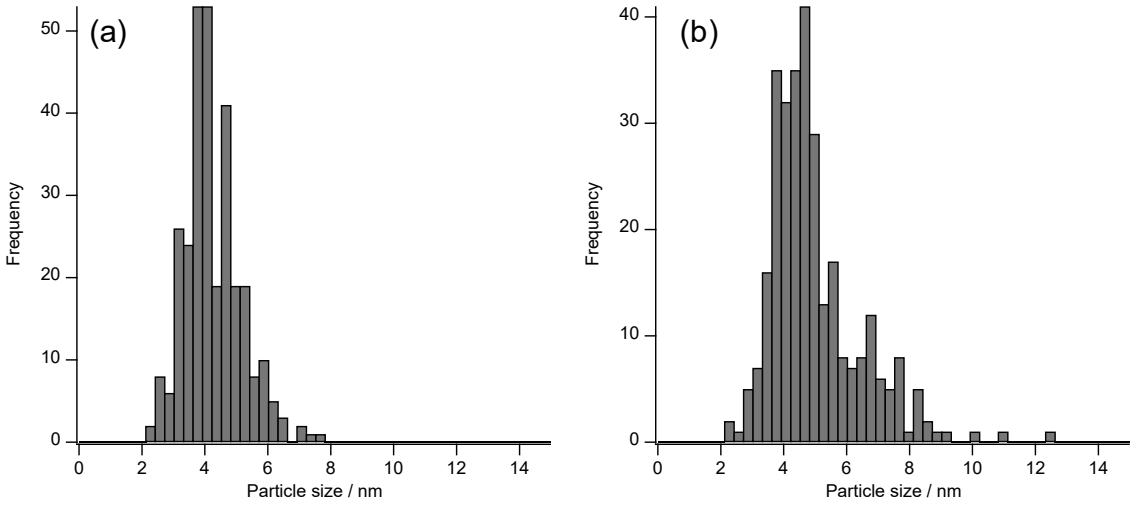

Figure 3-4. Pt NP size distribution of (a) Pt-MWCNT and (b) Pt–C subjected to 20,000-cycle ADT.

Vulcan, is extremely durable even in an O_2 atmosphere has been confirmed by our previous study that included the operando TEM observation of catalysts under low-humidity air conditions at 473 K.[71] If Pt NPs are moved onto such a stationary support by ADT, they would only be able to move along the grooves, as schematically shown in Figure 3-5. Consequently, the spherical Pt NPs on the SWCNT bundle were thought to acquire the nanorod shape when the NPs aggregated by colliding with each other. It is noteworthy that the Pt nanorod reportedly exhibited higher catalytic activity toward an ORR than the Pt nanoparticle because most of the surface of the former material has crystal planes providing higher catalytic activity like Pt(111).[143, 144] From this perspective, the spontaneous and advantageous shape change of the Pt NPs on the SWCNT bundle might explain the enhancement of the mass activity of the Pt-SWCNT after the ADT.

The Pt-MWCNT lost the mass activity after ADT, but its retention rate was considerably higher than that of the Pt–C. Evidently, the high durability of MWCNT must contribute to the retention of the catalytic activity. Because the MWCNT does not have bundle-forming properties, it was very hard to judge whether nanorod-shaped Pt was generated. However, it might be possible that the movement of the Pt NPs onto the stationary MWCNT surfaces changed some of their shapes to ones that were more suitable for an ORR.

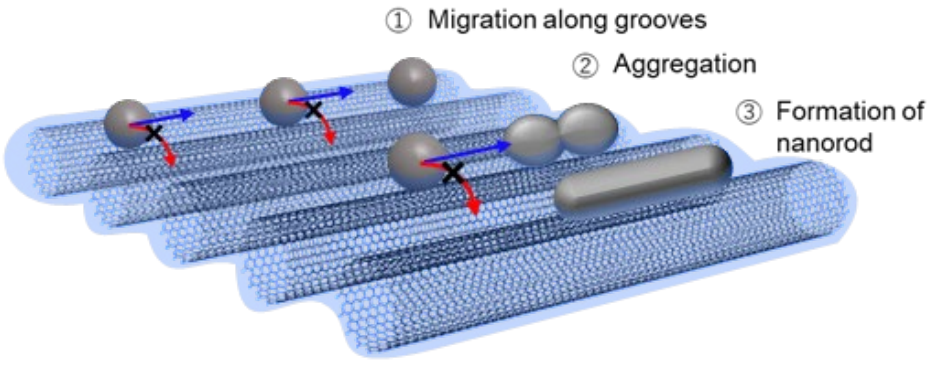

Figure 3-5. Schematic illustration of the plausible morphology variation mechanism of the Pt NPs supported on the SWCNT bundles during the ADT.

3-4. Conclusions

In conclusion, we have developed a straightforward method to prepare Pt NPs supported on CNTs using only two physical procedures, that is, sputtering Pt onto [dema][TfO] and then mixing it with CNTs at room temperature. The obtained electrocatalysts exhibit higher catalytic activity and durability than commercial Pt–C. Even if the performances of the Pt-SWCNT and Pt-MWCNT prepared in this study are compared with those of other Pt-CNTs prepared using chemical reactions, including the pre-treatment of CNTs in some cases, our catalysts certainly belong to the highest class, as demonstrated in Table 3-2. Of particular note is that the Pt-SWCNT prepared in this study maintained the highest mass activity after ADT, indicating high potential for its long-term use and reusability. As described in Chapter 2, the Pt NPs were immobilized on the CNTs by noncovalent bonding between Pt and CNTs, with protic IL acting as a nanoglue. The absence of direct bonding between Pt NPs and CNTs allowed the Pt NPs to migrate and aggregate with one another during ADT. In the case of the Pt-SWCNT, however, Pt NPs changed their shape to become nanorod-like due to their migration along grooves formed on the SWCNT bundle, resulting in a slight enhancement of the ORR activity. In general, particle growth should be prevented in fuel-cell engineering. However, the finding that the aggregation of particles in the Pt-SWCNT during the use of the catalyst results in an improvement in catalytic activity provides an innovative strategy for the design of ORR electrode catalysts.

Table 3-1. Performance comparison of Pt-NP-supported CNT reported in literatures

	CNT pretreatment	Immobilization of Pt NPs on CNT	ADT condition	ADT cycle number	Mean particle size /nm		ECSA /$m^2\ g_{Pt}^{-1}$		Mass activity /A g_{Pt}^{-1}		Specific activity /A m_{Pt}^{-2}		TOF** /$atom_{Pt}^{-1}\ sec^{-1}$		Reference
					Initial	After ADT	Initial	After ADT	Initial	After ADT	Initial	After ADT	Initial	After ADT	
Pt/MU-MWCNT	Unzipping CNT with potassium permanganate	Glycol reduction of Pt ion on CNT	Potential sweep, 0.6–1.1 V, 50 mV sec^{-1}	3000	1.95	-	103.4	82.2	174.5	93.3*	1.69	1.13	0.21	0.14	145
Pt@CNx/CNT	Coating CNT with polyaniline and pyrolyzing it	Chemical reduction of Pt ion at same time as aniline polymerization on CNT	Potential sweep, 0–1.2 V, 50 mV sec^{-1}	1500	3.1 ± 0.9	3.2 ± 0.7	74.3	77.0	111 (0.85 V)	108.5 (0.85 V)	1.5 (0.85 V)	1.41 (0.85 V)	0.19 (0.85 V)	0.18 (0.85 V)	87
PtNW/F-CNT	Sulfur-doping functionalized CNT by annealing with phenyl disulfide at 1000°C	Polyol reduction of Pt ion on sulfur-doped CNT with autoclave	Potential sweep, 0–1.5 V	3000	Nanowire	-	17.2	16.0	272 (0.9 V)	220 (0.9 V)	15.8 (0.9 V)	13.8 (0.9 V)	2.00 (0.9 V)	1.75 (0.9 V)	88
Pt/Ppy-MWCNT	Coating CNT with polypyrrole	Copolymerization of Pt complex and pyrrole on CNT	Square potential wave, 0.6 V (3 sec)–1.0 V (3 sec)	30000	1.5 ± 0.5	-	96.0	63.8*	166 (0.9 V)	124 (0.9 V)	1.7 (0.9 V)	1.9 (0.9 V)*	0.22 (0.9 V)	0.24 (0.9 V)	83
Pt/N-CNT	Coating CNT with Nafion	Polyol reduction of Pt ion on CNT	Potential sweep, 0.6–1.2 V, 100 mV sec^{-1}	6000	2.7	3.8	72.11	49.39	111 (0.9 V)	-	1.54 (0.9 V)	-	0.19 (0.9 V)	-	146
Pt-Gd(5/1)-MWCNT	Coating CNT with polypyrrole	Copolymerization of Pt complex, pyrrole and Gd complex on CNT	Square potential wave, 0.6 V (3 sec)–1.0 V (3 sec)	30000	1.6 ± 0.9	-	68.8	36	350 (0.9 V)	120 (0.9 V)	5.0 (0.9 V)	3.4 (0.9 V)	0.63 (0.9 V)	0.43 (0.9 V)	147
Pt-MWCNT	Nothing	Mixing Pt NP-dispersed IL and CNT at room temperature	Square potential wave, 0.6 V (3 sec)–1.0 V (3 sec)	20000	1.9 ± 0.3	4.2 ± 0.9	76.2	27.9	347.8 (0.9 V)	291.6 (0.9 V)	4.56 (0.9 V)	10.4 (0.9 V)	0.58 (0.9 V)	1.32 (0.9 V)	This work
Pt-SWCNT	Nothing	Mixing Pt NP-dispersed IL and CNT at room temperature	Square potential wave, 0.6 V (3 sec)–1.0 V (3 sec)	20000	1.9 ± 0.4	Nanorod (2.6 ± 0.8 /6.9 ± 3.6)	100.2	51.4	353.3 (0.9 V)	374.8 (0.9 V)	3.52 (0.9 V)	7.29 (0.9 V)	0.45 (0.9 V)	0.92 (0.9 V)	This work

*: calculated from a bar graph in the literature
**: TOF is given by

$$\mathrm{TOF}\ (\mathrm{atom}_{\mathrm{Pt}}^{-1}\,\mathrm{sec}^{-1}) = \frac{Specific\ activity\ (A\,m_{Pt}^{-2})}{4\ electron\ \times\ e\ (C\ electron^{-1})\ \times\ surface\ atom\ number\ (atoms_{Pt}\,m_{Pt}^{-2})}$$

where the average of the atomic density for Pt(111), Pt(110), and Pt(100) (1.50×10^{15}, 0.92×10^{15}, and 1.28×10^{15} [atom cm^{-2}], respectively) was used as the surface atom number.[148]

Chapter 4

Room-Temperature Fabrication of Electrocatalyst for Oxygen Reduction Using Pt Nanoparticle-dispersed Protic Ionic liquid with Poly(3,4-ethylenedioxythiophene)

4-1. Introduction

Chapter 2 and 3 described that a thin IL layer is present between the Pt-NPs and the carbon support. As one can suppose, however, the thin IL layer hampers for electron transfer between Pt-NPs and the carbon. As a deliberate method to solve this problem, an electropolymerizable compound was added in the IL and a conducting polymer network was formed in the IL layer by electrochemical oxidation.[72, 73] This strategy effectively works when using diphenyl amine and aniline as additives, but use of some other additives regrettably resulted in a failure; pyrrole and 3,4-ethylenedioxythiophene were decomposed when heated to induce Pt-NPs adsorption. Poly(3,4-ethylenedioxythiophene) (PEDOT) prepared by oxidative polymerization of the latter compound is known well as one of the ideal conducting polymers due to its attractive properties like high conductivity (up to 300 S cm^{-1}), high environmental stability, and flexibility, especially, when composited with poly(styrenesulfonate).[149-151]

Since a first invention as to adsorption of metal NPs onto carbon materials came from heating a mixture of the metal-sputtered IL and the carbon materials, heat treatment was considered inevitable. Quite recently, however, I found that adsorption of Pt-NPs on carbon nanotubes without heating was possible if protic IL was used, as described in Chapter 2 and 3. This desirable circumstance prompted us to use EDOT again as the electropolymerized additive in preparation of the Pt-NPs/C catalyst. Then, in the present study a Pt-NPs/C catalyst was

prepared by mixing protic IL containing EDOT and carbon black, and its electrocatalytic activity and durability were examined to confirm how the high-performance of PEDOT would be effective to improve the performance of the electrocatalyst.

4-2. Experimental section

4-2-1. Preparation of carbon-supported Pt nanoparticles catalysts

Preparation of Pt NPs dispersed [dema][TfO] by the ionic liquid-sputtering method was conducted in a similar manner to that described in Chapter 2. Subsequently, carbon black (3 mg, Vulcan XC-72) and 30 μL (2.8×10^{-4} mol) EDOT were added in the resulting Pt-NPs monodispersed [dema][TfO] (400 μL), and it was mixed with a planetary centrifugal mixer (Awatori-Rentaro AR-100, THINKY) at room temperature for 3 min. Then, the mixture was ultrasonically washed with *i*-propanol and centrifuged three times, followed by drying at 333 K under vacuum for 2 h. Hereafter, the obtained catalysts without and with EDOT are abbreviated as Pt-NPs/PIL/C and Pt-NPs/PIL+EDOT/C, respectively. A commercially available catalyst (Pt-NPs/C) (TEC10V30E, Tanaka Kikinzoku Kogyo K.K.) was used for comparison. The prepared catalysts was dispersed in a mixture of *i*-propanol and water (3:1, w:w) by ultrasonication to prepare an electrocatalyst ink.

4-2-2. Electrochemical analysis

Electrochemical measurement was carried out in the same method as in chapter 3. However, stability of the catalyst performance was examined by a start-stop test, which is one of the accelerated deterioration tests (ADT) proposed by Fuel Cell Commercialization Conference of Japan (FCCJ). The ADT was conducted by applying continuous potential sweeps between 1.0 V-1.5 V at 0.5 V s^{-1} to simulate the load applied at the start and stop of the fuel cell.[136]

4-3. Results and discussion

4-3-1. Electropolymerization of 3,4-ethylenedioxythiophene in [dema][TfO]

Since a formation of electronic network in a thin PIL layer as shown in Figure 4-1 is essential, electrochemical polymerization of EDOT in a [dema][TfO] layer was examined by cyclic voltammetry. An indium tin oxide (ITO) glass, on which an appropriate amount of [dema][TfO] dissolving 0.66 mol L^{-1} EDOT was put and spread, was used as a working electrode. This electrode was put in 0.1 mol L^{-1} $HClO_4$ together with a Pt counter electrode and an Ag/AgCl reference electrode. Of note, the thin PIL layer stably stayed on the ITO surface without dissolution in the electrolyte solution. Potential sweepings between 0.05 and 1.2 V vs. RHE at 50 mV s^{-1} gave cyclic voltammograms shown in Figure 4-2, in which pictures of the working

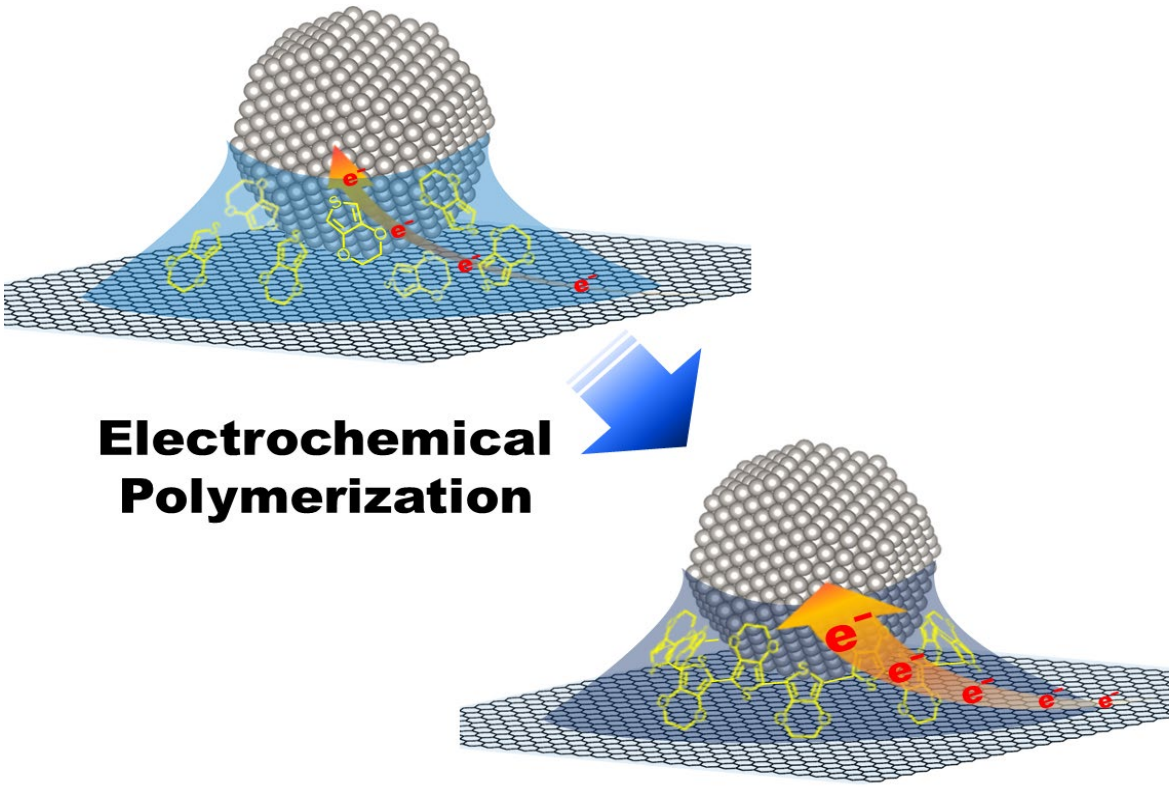

Figure 4-1. Schematic illustration of electrochemical polymerized EDOT in [dema][TfO] between Pt NP and carbon support.

electrode taken before and after electrochemical oxidation are also given. The voltammograms showed increase in oxidation currents at potentials positive of 0.9 V vs. RHE and steady increase in capacitive currents with potential cycles. The [dema][TfO] layer turned light blue and then deep blue at every positive potential sweep. At the same time, electrochromic behavior of fading at negative potentials was observed. Such the electrochemical behavior allowed us to

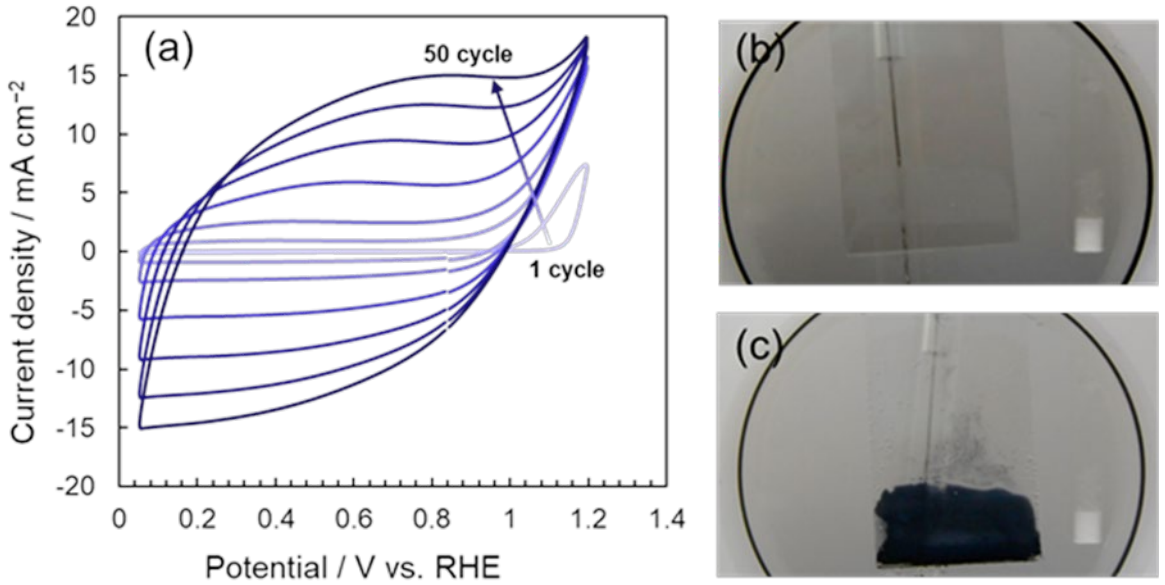

Figure 4-2. Cyclic voltammograms of ITO/[dema][TfO]+EDOT electrode taken in 0.1 M $HClO_4$ aqueous solution (a), and pictures of ITO/[dema][TfO]+EDOT electrode before (b) and after (c) the electropolymerization test.

confirm electrochemical polymerization of EDOT giving PEDOT in the [dema][TfO] layer.[152]

4-3-2. Characterization of carbon-supported Pt NPs

TEM images of Pt-NPs/PIL/C, Pt-NPs/PIL+EDOT/C, and commercial Pt-NPs/C, are shown in Figure 4-3. Although the former two samples were prepared at room temperature, the Pt nanoparticles were homogeneously immobilized on the surfaces of carbon black regardless of presence of EDOT in [dema][TfO]. Their mean particle sizes and loading amounts are given in Table 4-1 together with characteristic values as electrocatalysts that will be described later. The mean particle sizes estimated for Pt-NPs/PIL/C and Pt-NPs/PIL+EDOT/C were much

smaller than that for the commercial Pt-NPs/C. The Pt loading amount on Pt-NPs/PIL+EDOT/C was a little smaller than Pt-NPs/PIL/C. As described in Chapter 2 and 3, PIL can induce Pt adsorption on carbon materials even at room temperature, whereas use of ordinary IL requires heating at and over 200℃. From that point of view, the ability of PIL to

Table 4-1. Summary of particle size, loading amount, ECSA and mass activity.

	Mean particle size / nm	Loading amount of Pt / wt%	ECSA / $m_{Pt}^2\ g_{Pt}^{-1}$		Mass activity @ 0.9 V / A g_{Pt}^{-1}	
			Initial	After 20,000 cycle	Initial	After 20,000 cycle
Pt/C	3.7 ± 0.7	28.9	58.3	40.7	149.8	81.7
Pt/PIL/C	1.7 ± 0.3	22.7	59.2	50.0	277.2	198.5
Pt/PIL+EDOT/C	2.1 ± 0.3	10.3	71.6	63.4	328.3	227.1

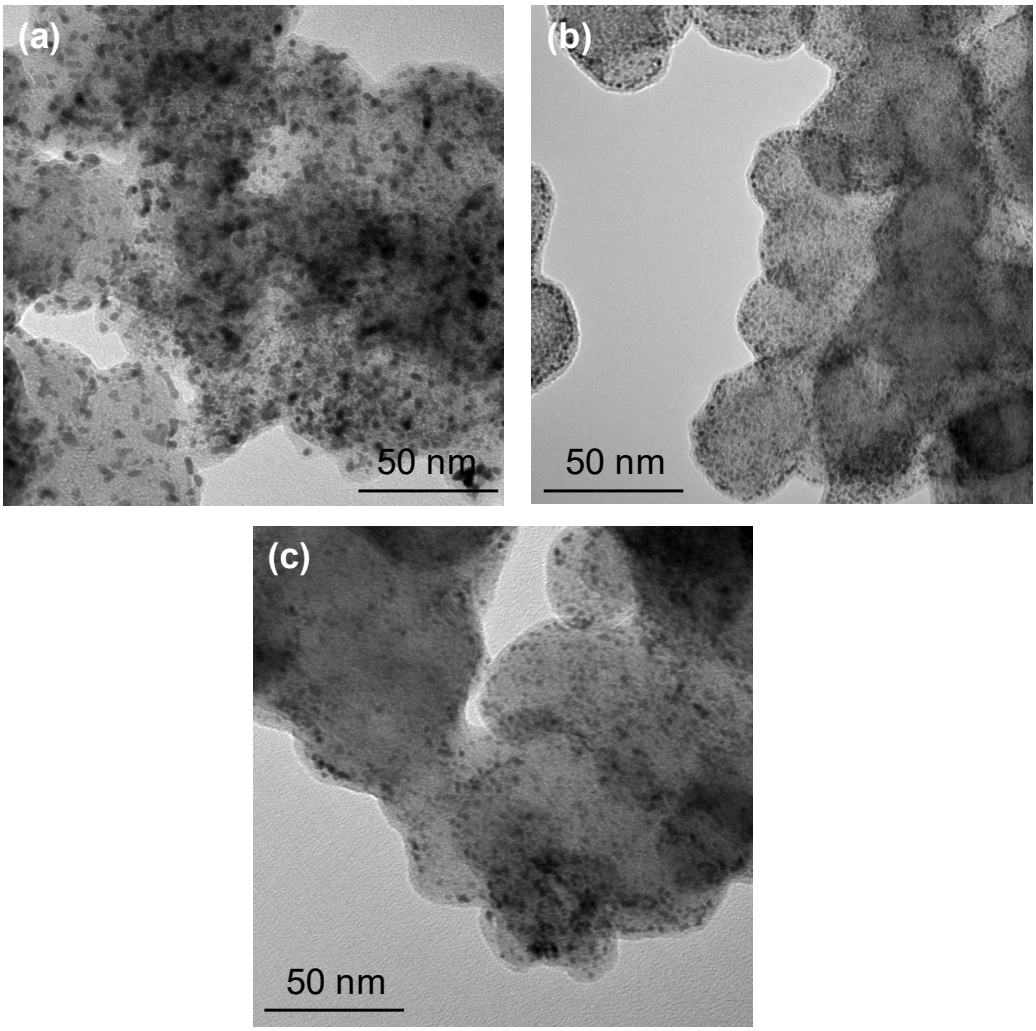

Figure 4-3. TEM images of (a) commercial Pt/C, (b) Pt/PIL/C and (c) Pt/PIL+EDOT/C.

bring about Pt adsorption even at room temperature might be slightly weakened by addition of EDOT in PIL. However, it was already confirmed that the Pt loading amount was tunable by changing the amount of Pt-NPs dispersed in IL.[70]

4-3-3. Electrocatalytic activities of carbon-supported Pt NPs

All catalysts exhibited the typical voltammograms of Pt including current peaks due to hydrogen adsorption/desorption and those due to oxidation of Pt surfaces and their reduction at negative and positive potential regions, respectively. The electrochemically active surface area (ECSA) of all Pt nanoparticles on each catalyst was estimated on basis of the electric charges required for the hydrogen adsorption/desorption on a polycrystalline Pt surface (210 $\mu C\ cm_{Pt}^{-2}$). The ECSA values of all catalysts and their retention rates, which are ratios of ECSA values at each cycle to the initial ones, are plotted as a function of cycle number, as shown in Figure 4-4(d). The Pt-NPs/PIL+EDOT/C kept apparently higher ECSA value than Pt-NPs/PIL/C and Pt-NPs/C during 20,000 cycles of ADT, indicating the significant effect of the conducting PEDOT network formed in the PIL layer on increasing the number of effectively functional Pt nanoparticles. The fact that both Pt-NPs/PIL+EDOT/C and Pt-NPs/PIL/C maintained higher retention rate than Pt-NPs/C strongly suggests that the existence of PIL between Pt-NPs and carbon supports functions for preventing the catalyst corrosion in a similar manner as the reports.[70, 71]

Figure 4-5(a) shows RDE polarization curves taken at 1,600 rpm for Pt-NPs/PIL/C, Pt-NPs/PIL+EDOT/C, and Pt-NPs/C catalysts in O_2-saturated 0.1 M $HClO_4$ before and after ADT. The electrocatalytic mass activities were evaluated from current values at 0.9 V vs. RHE and are given in Table 4-1. Apparently, the catalysts prepared with PIL exhibited higher catalytic activities than the commercial Pt-NPs/C catalyst. Surprisingly, the Pt-NPs/PIL+EDOT/C catalyst possessed over twice larger initial mass activity than the Pt-NPs/C catalyst, and then

1.5 times larger mass activity value than the initial mass activity of the Pt-NPs/C catalyst was kept even after 20,000 cycles of ADT. The laboratory to which I belong has previously reported enhancement of catalytic activitie by adding electropolymerizable compounds like aniline and diphenyl amine in Pt-sputtered IL, as mentioned in the 4-1 introduction section.[72, 73] Compared to the polymers of those compounds, PEDOT possesses the highest conductivity. This favorite characteristic resulted in the significant enhancement of the catalytic activity.

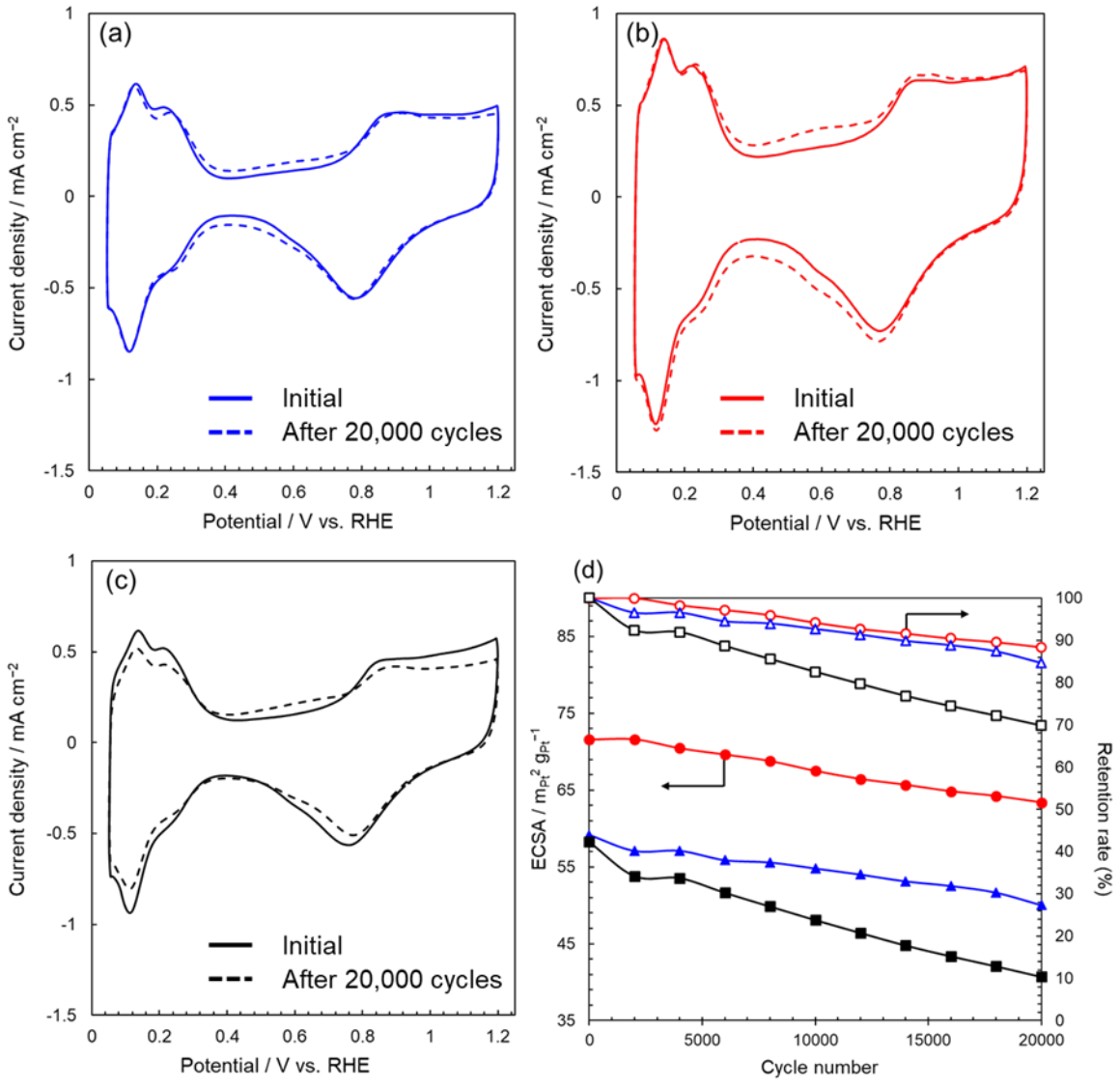

Figure 4-4. Cyclic voltammograms of (a) Pt-NPs /PIL/C, (b) Pt-NPs/PIL+EDOT/C and (c) commercial Pt-NPs/C taken before (solid lines) and after (broken lines) 20,000 cycles of ADT, and (d) ECSA values (filled marker) and their retention rates (unfilled marker) of Pt/C (black square), Pt-NPs /PIL/C (blue triangle) and Pt/PIL+EDOT/C (red circle).

To estimate optimized amount of EDOT in the Pt-sputtered PIL, the mass activities of Pt-NPs/PIL+EDOT/C containing different amount of EDOT were measured and the obtained values are plotted as a function of EDOT concentration, as shown in Figure 4-5(b). The concentration giving the highest mass activity was 0.66 mol L^{-1}, which corresponded 1 mol / 7.7 mol PIL. This molar ratio of EDOT in PIL should be appropriate for providing enough conductivity without giving unfavorable effects on Pt-NPs adsorption and catalytic activity at the Pt surfaces.

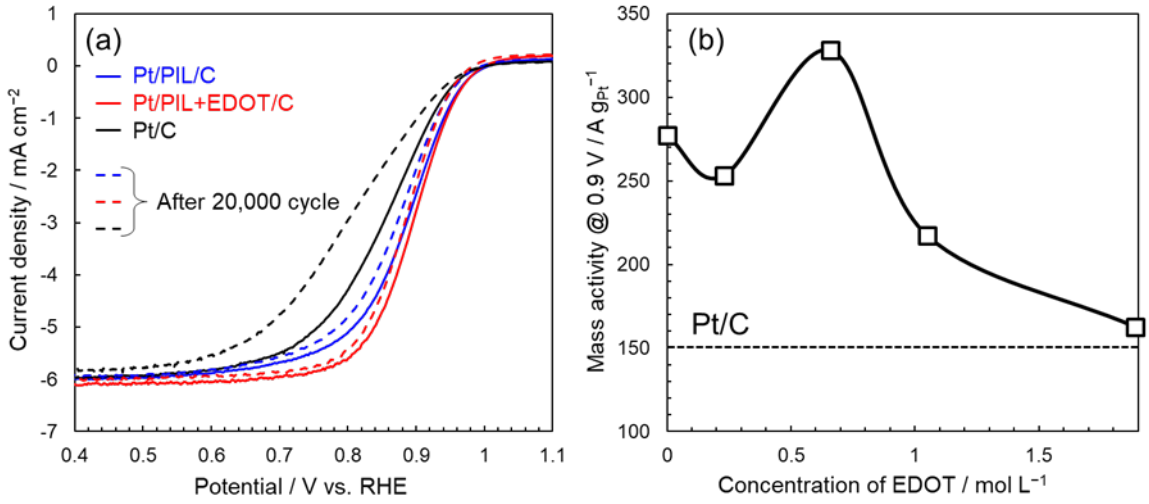

Figure 4-5. (a) RDE polarization curves of Pt-NPs/C (black), Pt-NPs/PIL/C (blue) and Pt-NPs/PIL+EDOT/C (red) at a scan rate of 10 mV s^{-1} taken before (solid lines) and after (broken lines) 20,000 cycles of ADT, and (b) mass activities of prepared catalysts with different amount of EDOT addition. A dash line indicates mass activity of Pt-NPs/C.

4-4. Conclusions

In conclusion, a novel method to fabricate carbon-supported Pt-NPs at room temperature, which is just mixing for 3 min of Pt-sputtered PIL including EDOT and carbon support, was successfully developed. The very thin PIL layer involving the conducting PEDOT network, which is present between Pt-NPs and carbon supports, makes the catalytic activity larger than that of the commercially available catalyst and makes it extremely durable against the accelerated deterioration tests. The preparation method that includes no chemical reactions except for the electrochemical polymerization during the initial cleaning would be the simplest among all methods to prepare the Pt-NPs/C electrocatalyst. It is expected that this method, which does not involve any wasteful materials, any by-products, and heating, is undoubtedly environmentally friendly and quite practical.

Summary

In this thesis, an innovative preparation method of high-performance electrocatalyst was developed by investigating a factor of effect on particle size in the “ionic liquid-sputtering method” and adsorption behavior of Pt NPs on carbon materials using IL. The main results and conclusions obtained in this thesis are summarized as follows:

In chapter 1, the effect of convection revealed by operando observation while conducting Au sputtering was described. It was found that Marangoni convection on interface between IL and vacuum caused by the gradient of surface tension was dominant in diffusion of Au cluster prepared in IL and affected particle size and distribution. As convection speed is changed by temperature and viscosity of IL etc., it is possible that the factors reported in previous research come down to convection of IL.

In chapter 2, the adsorption behavior of Pt NPs dispersed in IL onto carbon was described. IL made Pt NPs negative-charged by adsorption of anion, whereas [dema]-based protic IL among ILs made CNT positive-charged by [dema] cation adsorption. This opposite charge of Pt NPs and CNT induced electrostatic force between them and enabled preparation of the nanocomposite without heating. The CO stripping and XPS measurements indicated that there was no interaction between Pt NPs and CNT by IL canceling it.

In Chapter 3, the ORR activity of Pt NP-supported CNT prepared by the method proposed in chapter 2 was described. The obtained electrocatalysts showed about 2.5 times mass activity than commercial Pt/C. Interestingly, the ORR activity of Pt/PIL/SWCNT increased slightly even ADT of 20000 cycle because the shape of Pt nanoparticles after ADT became rod instead

of large particle by restricting migration of Pt nanoparticles to axial direction of SWCNT. This catalyst proposes a novel strategy to retain catalytic activity by not preventing migration but controlling the direction of migration because general strategies for maintaining ORR activity is to strongly immobilize Pt NPs on carbon support by polymer and chemical bond etc.

In Chapter 4, the effect of EDOT as additive on electrocatalytic performance was described. The electrocatalysts with EDOT in a thin IL layer was obtained because a new preparation method of Pt NP-supported carbon material using IL, which was only agitating at room temperature, was developed as described in Chapter 2 and 3. The very thin PIL layer involving the conducting PEDOT network, which was present between Pt-NPs and carbon supports, made the catalytic activity larger than that of the commercially available catalyst and made it extremely durable against the accelerated deterioration tests.

List of Publications

1. Operando Observation of Vacuum and Liquid Interface while Conducting Gold Sputtering onto Ionic Liquid for Preparation of Au Nanoparticles

   Tomoya Sasaki, Taro Uematsu, Tetsuya Tsuda and Susumu Kuwabata

   Electrochemistry, **2018**, *86(5)*, 223-225.

   DOI: 10.5796/electrochemistry.18-00039

2. Innovative Approach for Preparing Pt-Nanoparticle-Supported Carbon Nanotube Functional Electrocatalyst using Protic Ionic Liquids

   Tomoya Sasaki, Riki Takahashi, Reiko Izumi, Tetsuya Tsuda and Susumu Kuwabata

   ACS catalysis, under revision.

3. Room-Temperature Fabrication of Electrocatalyst for Oxygen Reduction Using Pt nanoparticle-dispersed Protic Ionic liquid with Poly(3,4-ethylenedioxythiophene)

   Tomoya Sasaki, Setsu Inoue and Susumu Kuwabata

   Electrochemistry, in press.

References

(1) Murphy, C. J.; Sau, T. K.; Gole, A. M.; Orendorff, C. J.; Gao, J.; Gou, L.; Hunyadi, S. E.; Li, T., *J. Phys. Chem. B* **2005,** 109, 13857-13870.

(2) Yang, Z. P.; Su, H. C., *Adv. Funct. Mater.* **2020,** 30, 1906788.

(3) Brasse, Y.; Gupta, V.; Schollbach, H. C. T.; Karg, M.; König, T. A. F.; Fery, A., *Adv. Mater. Interfaces* **2019,** 7, 1901678.

(4) Jia, C. J.; Schuth, F., *Phys. Chem. Chem. Phys.* **2011,** 13, 2457-2487.

(5) Soldevila-Barreda, J. J.; Metzler-Nolte, N., *Chem. Rev.* **2019,** 119, 829-869.

(6) Loza, K.; Heggen, M.; Epple, M., *Adv. Funct. Mater.* **2020,** 30, 1909260.

(7) Saha, K.; Agasti, S. S.; Kim, C.; Li, X.; Rotello, V. M., *Chem. Rev.* **2012,** 112, 2739-2779.

(8) Tan, L. L.; Wei, M.; Shang, L.; Yang, Y. W., *Adv. Funct. Mater.* **2020**.

(9) Ma, X.; He, S.; Qiu, B.; Luo, F.; Guo, L.; Lin, Z., *ACS Sens* **2019,** 4, 782-791.

(10) Buffat, P.; Borel, J. P., *Phys. Rev. A* **1976,** 13, 2287-2298.

(11) Ghosh Chaudhuri, R.; Paria, S., *Chem. Rev.* **2012,** 112, 2373-2433.

(12) Yang, L.; Shui, J.; Du, L.; Shao, Y.; Liu, J.; Dai, L.; Hu, Z., *Adv Mater* **2019,** 31, 1804799.

(13) Stamenkovic, V. R.; Mun, B. S.; Arenz, M.; Mayrhofer, K. J. J.; Lucas, C. A.; Wang, G. F.; Ross, P. N.; Markovic, N. M., *Nat. Mater.* **2007,** 6, 241-247.

(14) Li, Q.; Wu, L. H.; Wu, G.; Su, D.; Lv, H. F.; Zhang, S.; Zhu, W. L.; Casimir, A.; Zhu, H. Y.; Mendoza-Garcia, A.; Sun, S. H., *Nano Lett.* **2015,** 15, 2468-2473.

(15) Kuttiyiel, K. A.; Choi, Y.; Hwang, S.-M.; Park, G.-G.; Yang, T.-H.; Su, D.; Sasaki, K.; Liu, P.; Adzic, R. R., *Nano Energy* **2015,** 13, 442-449.

(16) Xiao, W.; Zhu, J.; Han, L.; Liu, S.; Wang, J.; Wu, Z.; Lei, W.; Xuan, C.; Xin, H. L.; Wang, D., *Nanoscale* **2016,** 8, 14793-14802.

(17) Jia, Q.; Caldwell, K.; Strickland, K.; Ziegelbauer, J. M.; Liu, Z.; Yu, Z.; Ramaker, D. E.; Mukerjee, S., *ACS Catal.* **2014,** 5, 176-186.

(18) Mezzavilla, S.; Baldizzonev, C.; Swertz, A. C.; Hodnik, N.; Pizzutilo, E.; Polymeros, G.; Keeley, G. P.; Knossalla, J.; Heggen, M.; Mayrhofer, K. J. J.; Schuth, F., *ACS Catal.* **2016,** 6, 8058-8068.

(19) Huang, X.; Zhao, Z.; Cao, L.; Chen, Y.; Zhu, E.; Lin, Z.; Li, M.; Yan, A.; Zettl, A.; Wang, Y. M., *Science* **2015,** 348, 1230-1234.

(20) Kitchin, J. R.; Norskov, J. K.; Barteau, M. A.; Chen, J. G., *Phys. Rev. Lett.* **2004,** 93, 156801.

(21) Rudi, S.; Tuaev, X.; Strasser, P., *Electrocatalysis* **2012,** 3, 265-273.

(22) Chan, K. Y.; Ding, J.; Ren, J. W.; Cheng, S. A.; Tsang, K. Y., *J. Mater. Chem.* **2004,** 14, 505-516.

(23) Cao, C.; Yang, G.; Dubau, L.; Maillard, F.; Lambert, S. D.; Pirard, J.-P.; Job, N., *Appl. Catal. B* **2014,** 150-151, 101-106.

(24) Kou, R.; Shao, Y.; Wang, D.; Engelhard, M. H.; Kwak, J. H.; Wang, J.; Viswanathan, V. V.; Wang, C.; Lin, Y.; Wang, Y.; Aksay, I. A.; Liu, J., *Electrochem. Commun.* **2009,** 11, 954-957.

(25) Grozovski, V.; Kasuk, H.; Nerut, J.; Härk, E.; Jäger, R.; Tallo, I.; Lust, E., *ChemElectroChem* **2015,** 2, 847-851.

(26) Wang, J.; Yin, G.; Liu, H.; Li, R.; Flemming, R. L.; Sun, X., *J. Power Sources* **2009,** 194, 668-673.

(27) Safo, I. A.; Oezaslan, M., *Electrochim. Acta* **2017,** 241, 544-552.

(28) Tsuda, T.; Hussey, C. L. In *Modern Aspects of Electrochemistry*, White, R. E., Ed. Springer Science+Business Media: New York, 2009; Vol. 45, pp 63-174.

(29) Ito, Y.; Nohira, T., *Electrochim. Acta* **2000,** 45, 2611-2622.

(30) Ohno, H., *Electrochemical Aspects of Ionic Liquids*. John Wiley & Sons, Inc.: New Jersey, 2005.

(31) Hagiwara, R.; Ito, Y., *J. Fluorine Chem.* **2000,** 105, 221-227.

(32) Itoh, T., *Chem. Rev.* **2017,** 117, 10567-10607.

(33) Handy, S. T., *Ionic Liquids - Classes and Properties*. InTech: Croatia, 2011.

(34) Brennecke, J. F.; Maginn, E. J., *AlChE J.* **2001,** 47, 2384-2389.

(35) Buzzeo, M. C.; Evans, R. G.; Compton, R. G., *ChemPhysChem* **2004,** 5, 1106-1120.

(36) Ueki, T.; Watanabe, M., *Macromolecules* **2008,** 41, 3739-3749.

(37) Kirchner, B., *Topics in Current Chemistry; Ionic Liquids*. Springer Science+Business Media: Heidelberg, Berlin, 2009.

(38) Walden, P., *Bull. Acad. Imper. Sci. St. Petersburg* **1914**, 405-422.

(39) Wilkes, J. S.; Levisky, J. A.; Wilson, R. A.; Hussey, C. L., *lnorg. Chem.* **1982,** 21, 1263-1264.

(40) Wilkes, J. S.; Zaworotko, M. J., *J. Chem. Soc., Chem. Commun.* **1992**, 965-967.

(41) Wegner, S.; Janiak, C., *Top. Curr. Chem.* **2017,** 375, 65.

(42) Vollmer, C.; Janiak, C., *Coord. Chem. Rev.* **2011,** 255, 2039-2057.

(43) Torimoto, T.; Tsuda, T.; Okazaki, K.; Kuwabata, S., *Adv Mater* **2010,** 22, 1196-1221.

(44) Dupont, J.; Fonseca, G. S.; Umpierre, A. P.; Fichtner, P. F.; Teixeira, S. R., *J. Am. Chem.*

Soc. **2002,** 124, 4228-4229.

(45) Endres, F.; el Abedin, S. Z., *Chem. Commun.* **2002**, 892-3.

(46) Steinrück, H.-P., *Surf Sci.* **2010,** 604, 481-484.

(47) Maier, F.; Niedermaier, I.; Steinruck, H. P., *J. Chem. Phys.* **2017,** 146, 170901.

(48) Lovelock, K. R.; Villar-Garcia, I. J.; Maier, F.; Steinruck, H. P.; Licence, P., *Chem. Rev.* **2010,** 110, 5158-90.

(49) Heller, B. S. J.; Lexow, M.; Greco, F.; Shin, S.; Partl, G.; Maier, F.; Steinruck, H. P., *Chemistry (Easton)* **2020,** 26, 1117-1126.

(50) Arimoto, S.; Kageyama, H.; Torimoto, T.; Kuwabata, S., *Electrochem. Commun.* **2008,** 10, 1901-1904.

(51) Chen, C.-Y.; Sano, T.; Tsuda, T.; Ui, K.; Oshima, Y.; Yamagata, M.; Ishikawa, M.; Haruta, M.; Doi, T.; Inaba, M.; Kuwabata, S., *Sci. Rep.* **2016,** 6, 36153.

(52) Tsuda, T.; Hosoya, K.; Sano, T.; Kuwabata, S., *Electrochim. Acta* **2019,** 319, 158-163.

(53) Hosoya, K.; Tsuda, T.; Kuwabata, S., *J. Power Sources* **2020,** 459, 228041.

(54) Torimoto, T.; Okazaki, K.-i.; Kiyama, T.; Hirahara, K.; Tanaka, N.; Kuwabata, S., *Appl. Phys. Lett.* **2006,** 89, 243117.

(55) Sugioka, D.; Kameyama, T.; Kuwabata, S.; Yamamoto, T.; Torimoto, T., *ACS Appl. Mater. Interfaces* **2016,** 8, 10874-10883.

(56) Liu, C.-H.; Mao, B.-H.; Gao, J.; Zhang, S.; Gao, X.; Liu, Z.; Lee, S.-T.; Sun, X.-H.; Wang, S.-D., *Carbon* **2012,** 50, 3008-3014.

(57) Suzuki, T.; Okazaki, K.-i.; Suzuki, S.; Shibayama, T.; Kuwabata, S.; Torimoto, T., *Chem. Mater.* **2010,** 22, 5209-5215.

(58) Foppa, L.; Luza, L.; Gual, A.; Weibel, D. E.; Eberhardt, D.; Teixeira, S. R.; Dupont, J., *Dalton Trans* **2015,** 44, 2827-34.

(59) Suzuki, S.; Morimoto, A.; Kuwabata, S.; Torimoto, T., *Jpn. J. Appl. Phys.* **2021,** 60.

(60) Torimoto, T.; Ohta, Y.; Enokida, K.; Sugioka, D.; Kameyama, T.; Yamamoto, T.; Shibayama, T.; Yoshii, K.; Tsuda, T.; Kuwabata, S., *J. Mater. Chem. A* **2015,** 3, 6177-6186.

(61) Akiyoshi, K.; Kameyama, T.; Yamamoto, T.; Kuwabata, S.; Tatsuma, T.; Torimoto, T., *RSC Adv.* **2020,** 10, 28516-28522.

(62) Luza, L.; Rambor, C. P.; Gual, A.; Alves Fernandes, J.; Eberhardt, D.; Dupont, J., *ACS Catal.* **2017,** 7, 2791-2799.

(63) Calabria, L.; Fernandes, J. A.; Migowski, P.; Bernardi, F.; Baptista, D. L.; Leal, R.; Grehl, T.; Dupont, J., *Nanoscale* **2017,** 9, 18753-18758.

(64) Wender, H.; de Oliveira, L. F.; Migowski, P.; Feil, A. F.; Lissner, E.; Prechtl, M. H. G.; Teixeira, S. R.; Dupont, J., *J. Phys. Chem. C* **2010,** 114, 11764-11768.

(65) Hatakeyama, Y.; Takahashi, S.; Nishikawa, K., *J. Phys. Chem. C* **2010,** 114, 11098-11102.

(66) Hatakeyama, Y.; Okamoto, M.; Torimoto, T.; Kuwabata, S.; Nishikawa, K., *J. Phys. Chem. C* **2009,** 113, 3917-3922.

(67) De Luna, M. M.; Gupta, M., *Appl. Phys. Lett.* **2018,** 112, 201605.

(68) Hatakeyama, Y.; Asakura, K.; Takahashi, S.; Judai, K.; Nishikawa, K., *J. Phys. Chem. C* **2014,** 118, 27973-27980.

(69) Hatakeyama, Y.; Onishi, K.; Nishikawa, K., *RSC Adv.* **2011,** 1, 1815-1821.

(70) Yoshii, K.; Tsuda, T.; Arimura, T.; Imanishi, A.; Torimoto, T.; Kuwabata, S., *RSC Adv.* **2012,** 2, 8262-8264.

(71) Yoshii, K.; Yamaji, K.; Tsuda, T.; Matsumoto, H.; Sato, T.; Izumi, R.; Torimoto, T.; Kuwabata, S., *J. Mater. Chem. A* **2016,** 4, 12152-12157.

(72) Izumi, R.; Yao, Y.; Tsuda, T.; Torimoto, T.; Kuwabata, S., *J. Mater. Chem. A* **2018,** 6, 11853-11862.

(73) Izumi, R.; Yao, Y.; Tsuda, T.; Torimoto, T.; Kuwabata, S., *Adv. Mater. Interfaces* **2018,** 5, 1701123.

(74) Yu, Y.; Luo, Z.; Yu, Y.; Lee, J. Y.; Xie, J., *ACS Nano* **2012,** 6, 7920-7927.

(75) Schatz, M. F.; Neitzel, G. P., *Annual Review of Fluid Mechanics* **2001,** 33, 93-127.

(76) Anderson, V. J.; Lekkerkerker, H. N., *Nature* **2002,** 416, 811-815.

(77) Hussain, S.; Erikson, H.; Kongi, N.; Sarapuu, A.; Solla-Gullón, J.; Maia, G.; Kannan, A. M.; Alonso-Vante, N.; Tammeveski, K., *Int. J. Hydrogen Energy* **2020,** 45, 31775-31797.

(78) Jukk, K.; Kongi, N.; Tammeveski, K.; Solla-Gullón, J.; Feliu, J. M., *ChemElectroChem* **2017,** 4, 2547-2555.

(79) Jukk, K.; Kongi, N.; Tammeveski, K.; Arán-Ais, R. M.; Solla-Gullón, J.; Feliu, J. M., *Electrochim. Acta* **2017,** 251, 155-166.

(80) Liu, M.; Zhao, Z.; Duan, X.; Huang, Y., *Adv Mater* **2019,** 31, e1802234.

(81) Borup, R.; Meyers, J.; Pivovar, B.; Kim, Y. S.; Mukundan, R.; Garland, N.; Myers, D.; Wilson, M.; Garzon, F.; Wood, D.; Zelenay, P.; More, K.; Stroh, K.; Zawodzinski, T.; Boncella, J.; McGrath, J. E.; Inaba, M.; Miyatake, K.; Hori, M.; Ota, K.; Ogumi, Z.; Miyata, S.; Nishikata, A.; Siroma, Z.; Uchimoto, Y.; Yasuda, K.; Kimijima, K.; Iwashita, N., *Chem. Rev.* **2007,** 107, 3904-3951.

(82) Ren, P.; Pei, P.; Li, Y.; Wu, Z.; Chen, D.; Huang, S., *Prog. Energy Combust. Sci.* **2020,** 80, 100859.

(83) Ichihashi, K.; Muratsugu, S.; Miyamoto, S.; Sakamoto, K.; Ishiguro, N.; Tada, M., *Dalton Trans* **2019,** 48, 7130-7137.

(84) Qi, Z.; Xiao, C.; Liu, C.; Goh, T. W.; Zhou, L.; Maligal-Ganesh, R.; Pei, Y.; Li, X.; Curtiss, L. A.; Huang, W., *J. Am. Chem. Soc.* **2017,** 139, 4762-4768.

(85) Zeng, S.; Lv, B.; Qiao, J.; Yang, W.; Zhu, C.; Zhang, Y.; Hu, D.; Chen, M.; Di, J.; Li, Q., *ACS Applied Nano Materials* **2019,** 2, 7870-7879.

(86) Yan, R.; Sun, X.; Zhang, X.; Zheng, J.; Jin, B., *Nanotechnology* **2020,** 31, 135703.

(87) Guo, L.; Jiang, W.-J.; Zhang, Y.; Hu, J.-S.; Wei, Z.-D.; Wan, L.-J., *ACS Catal.* **2015,** 5, 2903-2909.

(88) Hoque, M. A.; Hassan, F. M.; Jauhar, A. M.; Jiang, G.; Pritzker, M.; Choi, J.-Y.; Knights, S.; Ye, S.; Chen, Z., *ACS Sustainable Chemistry & Engineering* **2017,** 6, 93-98.

(89) Schneider, W. B.; Benedikt, U.; Auer, A. A., *Chemphyschem* **2013,** 14, 2984-2989.

(90) Ramos-Sanchez, G.; Balbuena, P. B., *Phys. Chem. Chem. Phys.* **2013,** 15, 11950-9.

(91) Saha, M. S.; Kundu, A., *J. Power Sources* **2010,** 195, 6255-6261.

(92) Alexeyeva, N.; Tammeveski, K.; Lopez-Cudero, A.; Solla-Gullón, J.; Feliu, J. M., *Electrochim. Acta* **2010,** 55, 794-803.

(93) Rajalakshmi, N.; Ryu, H.; Shaijumon, M.; Ramaprabhu, S., *J. Power Sources* **2005,** 140, 250-257.

(94) Xu, C.; Chen, J.; Cui, Y.; Han, Q.; Choo, H.; Liaw, P. K.; Wu, D., *Adv. Eng. Mater.* **2006,** 8, 73-77.

(95) Yu, R.; Chen, L.; Liu, Q.; Lin, J.; Tan, K.-L.; Ng, S. C.; Chan, H. S. O.; Xu, G.-Q.; Hor, T. S. A., *Chem. Mater.* **1998,** 10, 718-722.

(96) He, D.; Zeng, C.; Xu, C.; Cheng, N.; Li, H.; Mu, S.; Pan, M., *Langmuir* **2011,** 27, 5582-5588.

(97) Fujigaya, T.; Nakashima, N., *Adv Mater* **2013,** 25, 1666-1681.

(98) Okamoto, M.; Fujigaya, T.; Nakashima, N., *Small* **2009,** 5, 735-740.

(99) Tsuda, T.; Yoshii, K.; Torimoto, T.; Kuwabata, S., *J. Power Sources* **2010,** 195, 5980-5985.

(100) Upendar, S.; Mani, E.; Basavaraj, M. G., *Langmuir* **2018,** 34, 6511-6521.

(101) Baek, S.; Kim, J.; Kim, H.; Park, S.; Ban, H. W.; Gu, D. H.; Jeong, H.; Kim, F.; Lee, J.; Jung, B. M.; Choa, Y. H.; Kim, K. H.; Son, J. S., *ACS Appl. Mater. Interfaces* **2019,** 11, 11824-11833.

(102) Tsuda, T.; Kurihara, T.; Hoshino, Y.; Kiyama, T.; Okazaki, K.; Torimoto, T.; Kuwabata, S., *Electrochemistry* **2009,** 77, 693-695.

(103) Teliska, M.; Murthi, V. S.; Mukerjee, S.; Ramaker, D. E., *J. Phys. Chem. C* **2007,** 111, 9267-9274.

(104) Wand, P.; Bartl, J. D.; Heiz, U.; Tschurl, M.; Cokoja, M., *J. Colloid Interface Sci.* **2016,** 478, 72-80.

(105) Takasu, Y.; Iwazaki, T.; Sugimoto, W.; Murakami, Y., *Electrochem. Commun.* **2000,** 2, 671-674.

(106) Maillard, F.; Eikerling, M.; Cherstiouk, O. V.; Schreier, S.; Savinova, E.; Stimming, U., *Faraday Discuss.* **2004,** 125, 357-377.

(107) Arenz, M.; Mayrhofer, K. J.; Stamenkovic, V.; Blizanac, B. B.; Tomoyuki, T.; Ross, P. N.; Markovic, N. M., *J. Am. Chem. Soc.* **2005,** 127, 6819-6829.

(108) Ma, J.; Habrioux, A.; Guignard, N.; Alonso-Vante, N., *J. Phys. Chem. C* **2012,** 116, 21788-21794.

(109) Ma, J.; Habrioux, A.; Morais, C.; Lewera, A.; Vogel, W.; Verde-Gómez, Y.; Ramos-Sanchez, G.; Balbuena, P. B.; Alonso-Vante, N., *ACS Catal.* **2013,** 3, 1940-1950.

(110) Campos-Roldan, C. A.; Ramos-Sanchez, G.; Gonzalez-Huerta, R. G.; Vargas Garcia, J. R.; Balbuena, P. B.; Alonso-Vante, N., *ACS Appl. Mater. Interfaces* **2016,** 8, 23260-23269.

(111) Yan, X.; Suzuki, T.; Kitahama, Y.; Sato, H.; Itoh, T.; Ozaki, Y., *Phys. Chem. Chem. Phys.* **2013,** 15, 20618-20624.

(112) Cancado, L. G.; Pimenta, M. A.; Neves, B. R.; Dantas, M. S.; Jorio, A., *Phys. Rev. Lett.* **2004,** 93, 247401.

(113) Suzuki, H.; Kimura, T.; Yamamoto, G.; Hashida, T.; Motomiya, K.; Tohji, K.; Sato, Y., *RSC Adv.* **2017,** 7, 49917-49922.

(114) Isaifan, R. J.; Ntais, S.; Baranova, E. A., *Applied Catalysis A: General* **2013,** 464-465, 87-94.

(115) Garbarino, S.; Pereira, A.; Hamel, C.; Irissou, É.; Chaker, M.; Guay, D., *J. Phys. Chem. C* **2010,** 114, 2980-2988.

(116) Han, B.; Carlton, C. E.; Suntivich, J.; Xu, Z.; Shao-Horn, Y., *J. Phys. Chem. C* **2015,** 119, 3971-3978.

(117) Stamenkovic, V. R.; Fowler, B.; Mun, B. S.; Wang, G.; Ross, P. N.; Lucas, C. A.; Markovic, N. M., *Science* **2007,** 315, 493-497.

(118) Yano, H.; Kataoka, M.; Yamashita, H.; Uchida, H.; Watanabe, M., *Langmuir* **2007,** 23, 6438-6445.

(119) Karan, H. I.; Sasaki, K.; Kuttiyiel, K.; Farberow, C. A.; Mavrikakis, M.; Adzic, R. R.,

ACS Catal. **2012,** 2, 817-824.

(120) Gan, L.; Heggen, M.; Rudi, S.; Strasser, P., *Nano Lett.* **2012,** 12, 5423-5430.

(121) Li, Y.; Wang, Z. W.; Chiu, C. Y.; Ruan, L.; Yang, W.; Yang, Y.; Palmer, R. E.; Huang, Y., *Nanoscale* **2012,** 4, 845-851.

(122) Zhang, J.; Yang, H.; Fang, J.; Zou, S., *Nano Lett.* **2010,** 10, 638-644.

(123) Zhang, Z.; More, K. L.; Sun, K.; Wu, Z.; Li, W., *Chem. Mater.* **2011,** 23, 1570-1577.

(124) Bing, Y.; Liu, H.; Zhang, L.; Ghosh, D.; Zhang, J., *Chem. Soc. Rev.* **2010,** 39, 2184-2202.

(125) Reiser, C. A.; Bregoli, L.; Patterson, T. W.; Yi, J. S.; Yang, J. D.; Perry, M. L.; Jarvi, T. D., *Electrochem. Solid-State Lett.* **2005,** 8, A273-A276.

(126) Brightman, E.; Hinds, G., *J. Power Sources* **2014,** 267, 160-170.

(127) Shao-Horn, Y.; Sheng, W. C.; Chen, S.; Ferreira, P. J.; Holby, E. F.; Morgan, D., *Top. Catal.* **2007,** 46, 285-305.

(128) Dubau, L.; Castanheira, L.; Berthomé, G.; Maillard, F., *Electrochim. Acta* **2013,** 110, 273-281.

(129) Kinumoto, T.; Nishihira, H.; Matsuoka, M.; Eguchi, N.; Tsumura, T.; Toyoda, M., *Electrochemistry* **2015,** 83, 12-17.

(130) Eckardt, M.; Gebauer, C.; Jusys, Z.; Wassner, M.; Hüsing, N.; Behm, R. J., *J. Power Sources* **2018,** 400, 580-591.

(131) Hara, M.; Lee, M.; Liu, C.-H.; Chen, B.-H.; Yamashita, Y.; Uchida, M.; Uchida, H.; Watanabe, M., *Electrochim. Acta* **2012,** 70, 171-181.

(132) Speder, J.; Zana, A.; Spanos, I.; Kirkensgaard, J. J. K.; Mortensen, K.; Hanzlik, M.; Arenz, M., *J. Power Sources* **2014,** 261, 14-22.

(133) Castanheira, L.; Silva, W. O.; Lima, F. H. B.; Crisci, A.; Dubau, L.; Maillard, F., *ACS Catal.* **2015,** 5, 2184-2194.

(134) Willinger, E.; Tarasov, A.; Blume, R.; Rinaldi, A.; Timpe, O.; Massué, C.; Scherzer, M.; Noack, J.; Schlögl, R.; Willinger, M. G., *ACS Catal.* **2017,** 7, 4395-4407.

(135) Garsany, Y.; Baturina, O. A.; Swider-Lyons, K. E.; Kocha, S. S., *Anal. Chem.* **2010,** 82, 6321-8.

(136) Ohma, A.; Shinohara, K.; Iiyama, A.; Yoshida, T.; Daimaru, A., *ECS Trans* **2011,** 41, 775-784.

(137) Kuzume, A.; Herrero, E.; Feliu, J. M., *J. Electroanal. Chem.* **2007,** 599, 333-343.

(138) Chen, W.; Xiang, Q.; Peng, T.; Song, C.; Shang, W.; Deng, T.; Wu, J., *iScience* **2020,** 23, 101532.

(139) Shao, M.; Peles, A.; Shoemaker, K., *Nano Lett.* **2011,** 11, 3714-3719.

(140) Bharti, A.; Cheruvally, G., *J. Power Sources* **2017,** 360, 196-205.

(141) Toda, T.; Igarashi, H.; Uchida, H.; Watanabe, M., *J. Electrochem. Soc.* **1999,** 146, 3750-3756.

(142) Stamenkovic, V.; Mun, B. S.; Mayrhofer, K. J.; Ross, P. N.; Markovic, N. M.; Rossmeisl, J.; Greeley, J.; Norskov, J. K., *Angew. Chem. Int. Ed. Engl.* **2006,** 45, 2897-901.

(143) Xiong, X.; Liao, Y.; Du, C.; Luo, W.; Chen, S., *ChemElectroChem* **2016,** 3, 2281-2287.

(144) Chen, H. S.; Liang, Y. T.; Chen, T. Y.; Tseng, Y. C.; Liu, C. W.; Chung, S. R.; Hsieh, C. T.; Lee, C. E.; Wang, K. W., *Chem. Commun. (Camb.)* **2014,** 50, 11165-8.

(145) Shu, Q.; Xia, Z.; Wei, W.; Xu, X.; Sun, R.; Deng, R.; Yang, Q.; Zhao, H.; Wang, S.; Sun, G., *ACS Applied Energy Materials* **2019,** 2, 5446-5455.

(146) Wang, Q.; Dai, N.; Zheng, J.; Zheng, J. P., *J. Electroanal. Chem.* **2019,** 854.

(147) Ichihashi, K.; Muratsugu, S.; Matsui, H.; Higashi, K.; Sekizawa, O.; Uruga, T.; Tada, M., *J. Phys. Chem. C* **2020,** 124, 26925-26936.

(148) Paulus, U. A.; Wokaun, A.; Scherer, G. G.; Schmidt, T. J.; Stamenkovic, V.; Markovic, N. M.; Ross, P. N., *Electrochim. Acta* **2002,** 47, 3787-3798.

(149) Ouyang, J.; Chu, C. W.; Chen, F. C.; Xu, Q.; Yang, Y., *Adv. Funct. Mater.* **2005,** 15, 203-208.

(150) Snook, G. A.; Peng, C.; Fray, D. J.; Chen, G. Z., *Electrochem. Commun.* **2007,** 9, 83-88.

(151) Kayser, L. V.; Lipomi, D. J., *Adv Mater* **2019,** 31, 1806133.

(152) Groenendaal, B. L.; Jonas, F.; Freitag, D.; Pielartzik, H.; Reynolds, J. R., *Adv. Mater.* **2000,** 12, 481-494.

Acknowledgement

First of all, the author would like to express his sincerest gratitude to Prof. Dr. Susumu Kuwabata, Department of Applied Chemistry, Graduate School of Engineering, Osaka University, for his continuous guidance, many invaluable suggestions and warm encouragement throughout this work. The author would like to thank to Prof. Dr. Hidehiro Sakurai and Prof. Dr. Takahiro Kozawa for their reviewing this thesis with helpful comments and suggestions.

The author also wishes to express his special thanks to Associate Prof. Dr. Tetsuya Tsuda. The author would like to express her thanks to Assistant Prof. Dr. Taro Uematsu for many fruitful discussions, his valuable comments and suggestions, and a lot of helpful supports. The author is deeply grateful to Cross-Appointment Associate Prof. Dr. Hajime Matsumoto, Department of Energy Environment, Research Institute of Electrochemical Energy, National Institute of Advanced Industrial Science and Technology, for his valuable discussions and warm guidance. The author thanks secretary, Ms. Michiko Ebukuro and Ms. Miyuki Takahama for hearty supports. The author is indebted to Dr. Kei Hosoya, Mr. Yuya Uemura and Mr. Kohei Kumagai for their fruitful discussions and expert comments. The author is also grateful to all members of Kuwabata laboratory for their heartfelt encouragements and friendship.

The author would like to gratefully acknowledge Prof. Dr. Kenji Iijima, Ms. Yasuko Ueda, Ms. Miwa Shimizu and members of interactive materials science cadet program, and educational and financial assistance with deepest appreciation.

Finally, the author wishes to express her sincerest gratitude to his family, Machi Sasaki, Nariko Sasaki, Ken-ichi Sasaki and Yusuke Sasaki for their warm encouragement, hearty supports and continuous understanding.

June 2021

Tomoya Sasaki